Monthly Notices of the ROYAL ASTRONOMICAL SOCIETY

MNRAS **438,** 1630–1653 (2014) doi:10.1093/mnras/stt2309
Advance Access publication 2014 January 3

# Extended void merging tree algorithm for self-similar models

Esra Russell[1,2]★

[1]*Kapteyn Astronomical Institute, University of Groningen, PO Box 800, NL-9700 AM Groningen, the Netherlands*
[2]*Department of Mathematics, Izmir Institute of Technology, 35430 Gulbahcekoyu/Urla, Izmir, Turkey*

Accepted 2013 November 27. Received 2013 November 27; in original form 2013 September 1

**ABSTRACT**

In hierarchical evolution, voids exhibit two different behaviours related with their surroundings and environments, they can merge or collapse. These two different types of void processes can be described by the two-barrier excursion set formalism based on Brownian random walks. In this study, the analytical approximate description of the growing void merging algorithm is extended by taking into account the contributions of voids that are embedded into overdense region(s) which are destined to vanish due to gravitational collapse. Following this, to construct a realistic void merging model that consists of both collapse and merging processes, the two-barrier excursion set formalism of the void population is used. Assuming spherical voids in the Einstein-de Sitter Universe, the void merging algorithm which allows us to consider the two main processes of void hierarchy in one formalism is constructed. In addition to this, the merger rates, void survival probabilities, void size distributions in terms of the collapse barrier and finally, the void merging tree algorithm in the self-similar models are defined and derived.

**Key words:** methods: analytical – methods: numerical – cosmology: theory–large-scale structure of Universe.

## 1 INTRODUCTION

The present-day Universe shows a complex pattern of structures, called the Cosmic Web (Bond, Kofman & Pogosyan 1996). Galaxy redshift surveys find that voids are dominant features of the large-scale structure (Jõeveer, Einasto & Tago 1978; Kirshner et al. 1981; Geller & Huchra 1989; van de Weygaert 1991; Maurogordato, Schaeffer & da Costa 1992; Strauss et al. 1992; van de Weygaert & van Kampen 1993; da Costa et al. 1994; Fisher et al. 1995; Shectman et al. 1996; Einasto et al. 1997; Saunders et al. 2000; Plionis & Basilakos 2002; Jones et al. 2004; van de Weygaert & Bond 2008; van de Weygaert & Platen 2011). Differing from overdense haloes, voids evolve out of the underdensities in the primordial gravitational fluctuations. Due to their internal weak gravity driven by a negative density profile, they expand with respect to the background Universe rather than collapse. According to the void-based description of the cellular morphology of the Cosmic Web, voids are important components of hierarchical structure formation since the growth of the large-scale structure may be driven by the expansion of voids (Icke 1984; van de Weygaert 1991, 2003). In addition to this, numerical calculations and *N*-body simulations show that the voids tend to be spherical in time (Centrella & Melott 1983; Fujimoto 1983; Bertschinger 1985; Regos & Geller 1991; Dubinski et al. 1993; van de Weygaert & van Kampen 1993; Colberg et al. 2005; Tavasoli, Vasei & Mohayaee 2013) and this tendency is explained by the Bubble Theorem (Icke 1984).

Although there are differences between haloes and voids due to their origins, voids evolve hierarchically (Regos & Geller 1991; van de Weygaert & van Kampen 1993; Gottlöber et al. 2003; Sheth & van de Weygaert 2004; Colberg et al. 2005; Paranjape, Lam & Sheth 2012; Sutter et al. 2012a; Aragon-Calvo & Szalay 2013; Sutter et al. 2013) in a similar fashion to dark matter haloes. An important step towards understanding void hierarchy is provided by the void simulations of Dubinski et al. (1993) that are based on the analytical model of isolated spherical voids (Blumenthal et al. 1992). Another significant contribution is the work of Sahni, Sathyaprakah & Shandarin (1994). They applied the Lagrangian adhesion model description to the evolution of voids, resulting in revealing the unfolding void evolution. In their study, they found a strong correlation between the size of voids and the primordial gravitational potential at their centre. Another important result is shown in Sahni et al. (1994), Ceccarelli et al. (2013), Sutter et al. (2013); that large voids have more substructures than small size voids, and as voids grow older they become progressively emptier indicating less substructures within them. This result that voids have substructures is in agreement with *N*-body simulations, indicating that the interiors of voids are filled with subvoids, galaxies and even filaments

★ E-mail: esrarussell@iyte.edu.tr

(van de Weygaert & van Kampen 1993; Mathis & White 2002; Benson et al. 2003; Gottlöber et al. 2003). Sutter et al. (2013) point out that this tendency of a large void becoming emptier or erasing the substructures in itself is strongly related with choosing the tracking density in the simulations. As a result, a lower tracking density indicates less substructures in a void. The effect of these substructures on void evolution is important as they interact with their surroundings and have an impact on void evolution. Based on these theoretical and numerical results, Sheth & van de Weygaert (2004) point out that contrary to overdense regions, the evolution of voids is dictated by two processes depending on their environment: they can merge into larger voids and/or voids embedded in overdense regions can collapse. Ceccarelli et al. (2013) find a similar behaviour as Sheth & van de Weygaert (2004) in numerical simulations and classify voids into S (small)-Type and R (raising)-Type. Sheth & van de Weygaert (2004) suggest that the hierarchical evolution of these two different types of void processes can be described by the two-barrier excursion set formalism. Representing merging and collapsing dynamical behaviours of void populations, these two barriers encapsulate what it takes to let a void merge and collapse. In linear theory, the merging of a spherical void is represented by a constant critical density, $\delta_v = -2.81$ in the Einstein de Sitter (EdS) Universe, while the collapse of a spherical void is given by a fixed critical density value, $\delta_c = 1.686$. Later on, Furlanetto & Piran (2006) introduce an analytical model of void size in the galaxy distribution by applying the Extended Press Schechter (EPS) formalism. A numerical study of void hierarchy based on the Hierarchical Cosmic Spine method is introduced by Aragon-Calvo & Szalay (2013). Aragon-Calvo & Szalay (2013) apply this method to cosmological *N*-body simulation in order to analyse voids in hierarchical space. In their study, they stress out the importance of small-scale voids in order to obtain the dynamics around a halo. Based on the study of Sheth & van de Weygaert (2004), Russell (2013) construct a void merging tree algorithm of the growing spherical void population, based on the one-barrier excursion set theory as an adaption of the halo merging algorithm of Lacey & Cole (1993). Following up on Sheth & van de Weygaert (2004), Russell (2013) obtain an approximate analytical description of the merging tree based on excursion set theory, by assuming only growing spherical voids in the EdS Universe. This formalism leads to a considerably modified view of the evolution of voids. However, to define a more realistic void hierarchy model, it is essential to consider the dominant environmental influence on the evolution of voids by following Sheth & van de Weygaert (2004). Environmental influence strongly affects void sizes and their distribution. Following this, Sutter et al. (2013) provide a general framework in order to make connections between dark matter voids and galaxy voids from the same cosmological simulation by using the hierarchical tree structure of voids.

The different aspects of void populations have been discussed by observational and numerical studies (Regos & Geller 1991; Dubinski et al. 1993; van de Weygaert & van Kampen 1993; El-Ad, Piran & Dacosta 1997; Plionis & Basilakos 2002; Gottlöber et al. 2003; Benson et al. 2003; Hoyle & Vogeley 2002, 2004; Colberg et al. 2005; Tikhonov & Karachentsev 2006; Colberg et al. 2008; Kraan-Korteweg et al. 2008; Tully et al. 2008; Tinker & Conroy 2009; Lavaux & Wandelt 2010; Kreckel, Joung & Cen 2011; Bos et al. 2012; Lavaux & Wandelt 2012; Kreckel et al. 2012; Pan et al. 2012; Sutter et al. 2012a,b; Aragon-Calvo & Szalay 2013; Beygu et al. 2013; Tavasoli et al. 2013). Today we know that the void size range is approximately 5–135 $h^{-1}$ Mpc (Sutter et al. 2012a). However, there are some studies claiming that voids can have very small sizes, 0.7–3.5 $h^{-1}$ Mpc (Karachentsev et al. 2004; Tikhonov & Karachentsev 2006; Tikhonov & Klypin 2009). Based on these studies, Tikhonov et al. (2009) compare the observed spectrum of minivoids in the local volume within an 8 Mpc size sphere in the Local Group with the spectrum of minivoids determined from the simulations in the cold dark matter (CDM) and warm dark matter (WDM) models. They show the difference between the observed spectra of minivoids in the ΛWDM and ΛCDM models. Viel, Colberg & Kim (2008) make a preliminary attempt to link the population of voids in the transmitted Lyman $\alpha$ flux to the underlying gas density, temperature and dark matter density. The use of Lyman $\alpha$ high-resolution spectra is important in the sense that it explores a new regime at scales, redshifts and densities which are currently not probed by other observables: the scales are of the order of a few to tens of Mpc, the redshift range is between $z = 2$ and 4, while the densities are around the mean density.

There are more attempts to understand the dynamical, thermal and chemical evolution of the void population, and the interplay between galaxies and the intergalactic medium (D'Aloisio & Furlanetto 2007; Shang, Crotts & Haiman 2007). Motivated by the empirical evidence for significant pre-heating of at least parts of the intergalactic medium at $z \sim 3$, Shang et al. (2007) make a simple model for the spatial distribution of pre-heated regions. The model assumes spherical ionized bubbles around collapsed dark matter haloes and allows these spheres to merge into larger superbubbles. The number of voids that such ionized bubbles would produce in Lyman $\alpha$ absorption spectra of background quasars is predicted. D'Aloisio & Furlanetto (2007) present analytic estimates of galaxy void sizes at redshifts $z \sim$ 5–10 using the excursion set formalism. Another interesting study on void excursions addresses the issue of void formation in modified gravity models. Some of these involve a scalar field that couples to matter and introduces a fifth force. This force leads to a universal enhancement of gravity (Farrar & Peebles 2004; Gubser & Peebles 2004a,b), (Farrar & Rosen 2007; Brookfield, van de Bruck & Hall 2008; Hellwing & Juszkiewicz 2009; Clampitt, Cai & Li 2013). Clampitt et al. (2013) investigate the fifth force in voids in chameleon models by using void statistics based on the excursion set formalism. They point out that driven by the outward pointing fifth force, individual voids in chameleon models expand faster and grow larger than voids in the ΛCDM Universe.

In this study, a model is formulated to construct a merger tree formalism consisting of collapse and merging processes as an extension of the growing void merging tree of Russell (2013) by treating the void in cloud problem. In this model, the size of voids by using recent void catalogues is defined and a void merging tree formalism is obtained taking into account the merging process of void populations as well as the collapse process. To do this, the Lacey and Cole merging tree algorithm (Lacey & Cole 1993) of dark matter haloes in the EdS universe for spherical voids is adopted. Since the Lacey and Cole merging tree algorithm (Lacey & Cole 1993) of dark matter haloes provides an approximated dark matter solutions, in this study we only focus on the self-similar spectra to construct a void merging algorithm. As a result, the new void merging tree algorithm is extended to the two-barrier excursion set formalism in order to describe void merging and collapse in one model in the self-similar models.

## 2 COSMOLOGY

In this section, the normalization of the cosmological models is explained. These models are used in the two-barrier excursion set to obtain the quantities used for the void merging tree. Here, the power-law power spectra are taken into account with different spectral index and these spectra are approximated to a favoured ΛCDM by following Sheth & van de Weygaert (2004). The normalization of the spectra in the self-similar models is relatively easier to calculate given the form of the power spectrum,

$$P(k) \approx k^n, \tag{1}$$

where $n$ refers to the spectral index or the slope of the power spectrum. The variance of the self-similar spectra as a function of mass, volume and size is given by

$$\sigma^2(M) = S(M) = {\delta^2}_v \left(\frac{M}{M_*}\right)^{-\alpha} = \delta_v^2 \left(\frac{V}{V_*}\right)^{-\alpha} = {\delta^2}_v \left(\frac{R}{R_*}\right)^{-3\alpha}, \tag{2}$$

in which $\alpha$ is defined as $(n + 3)/3$. Here, $M_*$, $V_*$ and $R_*$ are the characteristic mass, volume and radius. The characteristic mass of the self-similar spectra is given by

$$M_*(z) = \left(\frac{\sigma_8}{|\delta_v|}\right)^{6/n+3}. \tag{3}$$

To normalize the self-similar power spectra, the mass function in mass variance in equation (2) is chosen as $M = M_*$. Hence, the characteristic mass variance is equal to the linear underdensity $\sigma^2(M_*) \sim |\delta_v|$. By following this definition of characteristic mass in equation (2), the comoving radius $R$ of a void region for self-similar models is given by Sheth & van de Weygaert (2004),

$$R = R_* \left(\frac{\sigma_8}{|\delta_v|}\right)^{2/n+3}. \tag{4}$$

Note that in our calculations, the characteristic void size is chosen as $R_* = 8\ h^{-1}$ Mpc in the self-similar models. This allows us to fix the variance $\sigma$ at the scale $M = M_*$. Then, the void excursion set of the toy models is obtained in terms of physical scales.

In this study, spherical contraction and expansion representing the collapse and merging void processes are taken into account. These dynamical processes are described with respect to linear theory. According to linear theory, an object of linear density $\delta$ will collapse or shellcross at redshift $z$ when its value dominates $\delta_c(z)$ or $\delta_v(z)$,

$$\delta_c(z) = \frac{\delta_c(0)}{D(z)} = \delta_c(0)\,(1 + z) \tag{5}$$

$$\delta_v(z) = \frac{|\delta_v(0)|}{D(z)} = |\delta_v(0)|\,(1 + z)\,, \tag{6}$$

where $\delta_c(z = 0) = 1.686$ and $\delta_v(z = 0) = -2.81$ are the linearly extrapolated densities in the linear regime. Note that the growth factor $D(z)$ encapsulates the geometry of the collapsing/expanding objects to denote the linear density perturbation. The growth factor normalized to the present-day Universe $D(z = 0) = 1$. In linear theory, the growth factor $D(z)$ has the same form for overdense and underdense regions, which is $D(z) = 1/(1 + z)$ in the EdS Universe. Here, by taking into account the fact that the shellcrossing and collapse barriers are only redshift dependent in the EdS Universe as defined in equations (5) and (6), the linear densities are used as time variables following the algorithm of Lacey & Cole (1993).

## 3 TWO BARRIER EPS FORMALISM

The analytical evaluation of the two-barrier random walk problem takes into account a distribution function $f_v(M)$ on a mass scale $M$ (Sheth & van de Weygaert 2004),

$$f_v(M)\,\mathrm{d}M \approx \frac{1}{\sqrt{2\pi}} \frac{\nu_v}{\sigma^2} \exp\left[-\frac{\nu_v^2}{2}\right] \exp\left[-\frac{|\delta_v|}{\delta_c}\frac{\Upsilon^2}{4\nu_v^2} - \frac{2\Upsilon^4}{\nu_v^4}\right] \mathrm{d}M, \tag{7}$$

corresponding to a fractional underdensity function $\nu_v(M)$ which is defined as

$$\nu_v(M) \equiv \frac{\delta_v}{\sigma(M)} = \frac{\delta_v}{\sqrt{S}}, \tag{8}$$

where $\delta_v$ is the void threshold density, the mass variance function is $\sigma(M)$ and the mass scale function is $S$. In equation (7) $\Upsilon$ is the void and cloud parameter. It is defined as

$$\Upsilon \equiv \frac{|\delta_v|}{(\delta_c + |\delta_v|)}. \tag{9}$$

The void and cloud parameter $\Upsilon$ has a key importance, since it shows the effect of the overdense regions/haloes on the void population. Therefore, the mass fraction equation (7) represents the hierarchical evolution of voids that are dominated by two different behaviours: merging or collapsing. These two behaviours are represented by two barriers in the excursion set formalism; the merging barrier is defined

by the linear collapse $\delta_c$ and shellcrossing $\delta_v$ densities. Since void and cloud parameter $\Upsilon$ is a time-dependent function and consists of the ratio of the barriers, it is rearranged as

$$\Upsilon = \frac{1}{\gamma(z_c, z_v) + 1}, \qquad \gamma(z_c, z_v) \equiv \frac{\delta_c(z_c)}{|\delta_v(z_v)|}, \qquad \gamma(z_c, z_v) = \frac{\delta_{c0}}{|\delta_{v0}|}\frac{1+z_c}{1+z_v}, \tag{10}$$

and a new parameter $\gamma$ is defined which is the barrier ratio $\delta_c/|\delta_v|$. For a given collapse redshift $z_c$ when collapse happens and a shell crossing redshift $z_v$ when merging occurs, the parameter $\gamma$ becomes constant. Note that the mass fraction function can be transformed into mass, volume or size scales by following Sheth & van de Weygaert (2004),

$$f_v(S)\,\mathrm{d}S \propto f_v(M)\,\mathrm{d}M = f_v(V)\,\mathrm{d}V \propto f_v(R)\,\mathrm{d}R.$$

This leads us to construct void evolution in terms of volume $S(V)$ and size scales $S(R)$ implicitly. Considering this and substituting the barrier ratio by using equation (10) in the two-barrier mass distribution equation (7), the distribution function is obtained in terms of volume/size scale as follows,

$$f_v(S)\,\mathrm{d}S \approx \frac{1}{\sqrt{2\pi}}\frac{\delta_v}{S^{3/2}}\exp\left(-\frac{\delta_v^2}{2S}\right)\exp\left(-\frac{1}{4}\frac{1}{\gamma}\frac{1}{(1+\gamma)^2}\frac{S}{\delta_v^2} - 2\frac{1}{(1+\gamma)^4}\frac{S^2}{\delta_v^4}\right)\mathrm{d}S. \tag{11}$$

The volume/size distribution equation (11) shows the hierarchical evolution of voids that are dominated by two processes; merging and collapsing in terms of the EPS formalism. Fig. 1 illustrates the two main void processes in the context of the EPS formalism. As is seen from the figure, a spherical void with volume scale $S_1 = S(V_1)$ starts its evolution at barrier $\delta_{v_1}$ and its volume grows due to a merging event when the random walk of the density function crosses a new barrier $\delta_{v_2}$ with volume scale $S_2 = S(V_2)$ $(V_2 > V_1)$. At this point, the void processes are classified into two main groups. The first one is the void merging/growing gradually. According to this, there are two possible scenarios to explain a gradual merging event: (i) if a void is not embedded in an overdense region, it will merge gradually (lower red line in Fig. 1), or an embedded void is large enough that it is not affected by collapse regions. This indicates that in the context of the two-barrier formalism, the collapse barrier is larger than the shell crossing barrier ($\delta_c \gg \delta_v$, which leads to the collapse barrier moving to $\delta_c \to \infty$) (upper red line in Fig. 1). In Fig. 1, the second void process is void collapse. The random walk of voids that are of a relatively small size compared to their large volume counterparts, merge until reaching the collapse barrier $\delta_c$ and when they reach this barrier they are squeezed at overdense boundaries and collapse under gravitational collapse (black lines). These two evolutionary paths can be described in terms of the barrier ratio or void in cloud parameter since these parameters have the key importance of indicating which process is dominant over the other one. When the value of the overdense barrier $\delta_c$ becomes higher than the underdense barrier $\delta_c \gg \delta_v$ or $\delta_c \to \infty$, the barrier ratio becomes infinite, which makes the void and cloud parameter zero, $\Upsilon \to 0$. Due to this fact, the second exponential term in equation (11) disappears. This means that the contribution of embedded/minor voids in the distribution equation (11) is unimportant. At this limit, the two-barrier distribution reduces to a single barrier at $\delta_v$ and then the abundance of voids is given by the void in void process which is analogous to the cloud in cloud process (Sheth & van de Weygaert 2004; D'Amico et al. 2011; Russell 2013). Fig. 2 shows the distribution function of the scaled density with respect to different barrier ratio parameters $\gamma$. As is seen for larger values $\gamma \gg 0.5$, the mass fraction function approach to the void in void problem of the one-barrier excursion set, indicates a gradually merging void process. However, the void distribution function with the barrier ratio $\gamma \leq 0.5$ has more contributions from the embedded voids, which leads to the void in cloud problem. In this case, the distribution function

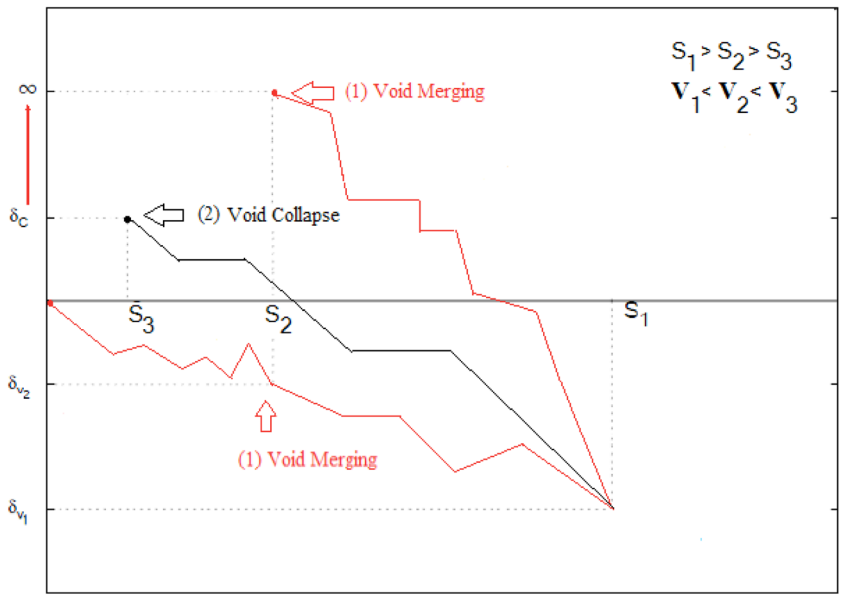


**Figure 1.** Illustration of the excursion set theory formalism representing two important void processes in terms of volume scales and two barriers; collapse $\delta_c$ and shellcrossing $\delta_v$. The void merging and collapse processes are indicated by red and black lines.

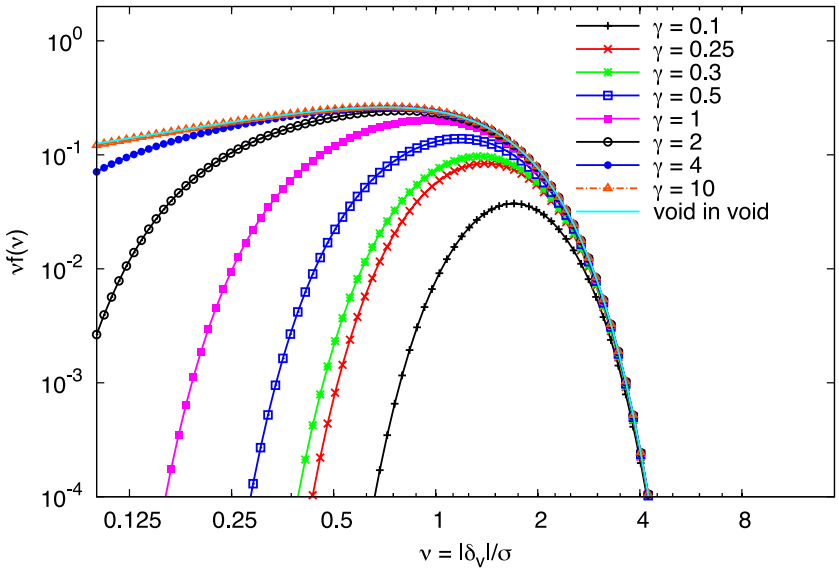


**Figure 2.** The scaled fraction of the void population in terms of different barrier ratios $\gamma$. When the ratio increases $\delta_c \gg \delta_v$, the distribution turns into the void in void distribution (most upper line) in the limit of $\gamma = 10$. When the ratio value reaches $\gamma = 0.5$ or higher values than this, the distribution is well peaked around the characteristic mass $\nu = 1$ ($\sigma = |\delta_v|$).

shows two cut-offs at small and large fractional underdensities $\nu$, in other words at small and large void volumes, indicating embedded voids are unlikely to have volumes larger or smaller than these cut-off values. Sheth & van de Weygaert (2004) point out that the distribution function is well peaked around $v \sim 1$ ($\sigma \sim |\delta_v|$) for the barrier ratio $\gamma \geq 0.25$. They also mention that the distribution function is not correct for the barrier ratio $\gamma \leq 0.25$. These basic descriptions and formulations frame the centre of this paper. Here, the main goal is to construct a void merging algorithm that takes into account the two void processes into one hierarchical model by using the two-barrier volume/size distribution function of Sheth & van de Weygaert (2004) based on the excursion set formalism.

Before giving the details of the void merging algorithm based on the two-barrier excursion set, it is crucial to treat the void in cloud problem in the context of excursion set theory. The problem of the void in void process is based on the derivation of the EPS formalism. The EPS formalism is a random walk (Brownian motion) excursion process that is conditioned to be positive $\delta > 0$ in terms of increasing scales $S$. Here, a problem arises in the void in cloud process, in that random trajectories of this process change from positive $\delta > 0$ to negative $\delta < 0$ values with increasing scales $S$. In other words, random trajectories of a void in cloud process make their first crossing at a negative barrier, then by crossing $\delta = 0$, reach the positive collapse barrier (see void collapse random walk in Fig. 1).

In the following subsection, a simple method is introduced based on the idea of constructing a sequence of random walks converging almost entirely to a Brownian motion (Marchal 2003). This simple method allows us to treat the complex evolution of the void processes in the EPS theory based on the scaled void distribution function.

### 3.1 Method to treat void in cloud problem

Here, the definition of Brownian motion and its classification are briefly introduced. Then, the interpretation of this classification is shown in terms of the EPS formalism. After defining the random walk property of the void in cloud, the details of the method and then application of this simple method to the two-barrier void distribution are given in order to obtain a merging algorithm of void populations based on the halo merging algorithm of (Lacey & Cole 1993, hereafter LC93).

Press & Schechter (1974) derive an analytical formalism to infer the number density of collapsed objects at a given redshift and mass interval based on combining Gaussian statistics of the linearly extrapolated density field with the non-linear evolution described by the spherical model. However, their formalism indicates a problem that is named as the cloud in cloud problem since they did not take into account low-density areas representing small embedded structures. Bond et al. (1991) propose a solution to this problem by taking into account the probability that a subsequent filtering of larger scales results in having linear density contrast larger than the collapse barrier $\delta > \delta_c$ at some point. Bond et al. (1991) identify the mass fraction of matter in virilized objects with mass greater than $M$ in which the initial density contrast lies above a critical overdensity when smoothed on some filter of radius greater than or equal to $R_f(M)$. The mass density function is then given by the rate of first upcrossing of the critical overdensity level as one decreases $R_f$ at a constant position $R$ (Bond et al. 1991). The shape of the mass function depends on the choice of filter function. The simplest case is sharp-$k$ space filtering, in which the field performs a *Brownian random walk* as each increment to $\delta(S)$ when $S$ is increased, which comes from a new set of Fourier modes in a thin spherical shell in $k$-space. Thus, for a Gaussian random field it is not correlated with any of these previous steps. As a consequence of this, these trajectories $\delta(S)$ are governed by a simple diffusion equation in which $\delta(S)$ increases with $S$.

### 3.2 Brownian random walk characteristics

Here, the definition and properties of a Brownian random walk are given in terms of the EPS formalism.

*Definition.* A standard (one-dimensional) Brownian motion with respect to a filtration $R_f$ is a collection of random variables $\delta(S)$, $S \geq 0$ satisfying the following (Pitman 1999):

(i) $\delta(S = 0) = 0$;
(ii) if $S' < S$, then $\delta(S) - \delta(S')$ is a measurable random variable, independent of the previous increment, with a Gaussian distribution;
(iii) with probability one, $S \mapsto \delta(S)$ is a continuous function.

There are three characteristics of the Brownian random walk; bridge, excursion and meander.
*Theorem.* There exists a family of random walks in the interval [0, $S$] where all numbers in the interval are integers for every $S$ (Marchal 2003).

(i) A Brownian bridge is defined as a random walk of cumulative density contrast $\delta(S)$ which has length $S$ and is conditioned to return to 0 at scale $S$ in the interval (Fig. 3). In the EPS formalism, a Brownian bridge can be described as minima of the excursion characteristic with negative barriers which form underdense regions.
(ii) A Brownian excursion is defined as a cumulative random walk of density contrast, $\delta(S)$ which has length $S$ and is conditioned to stay positive in the interval (Fig. 3).

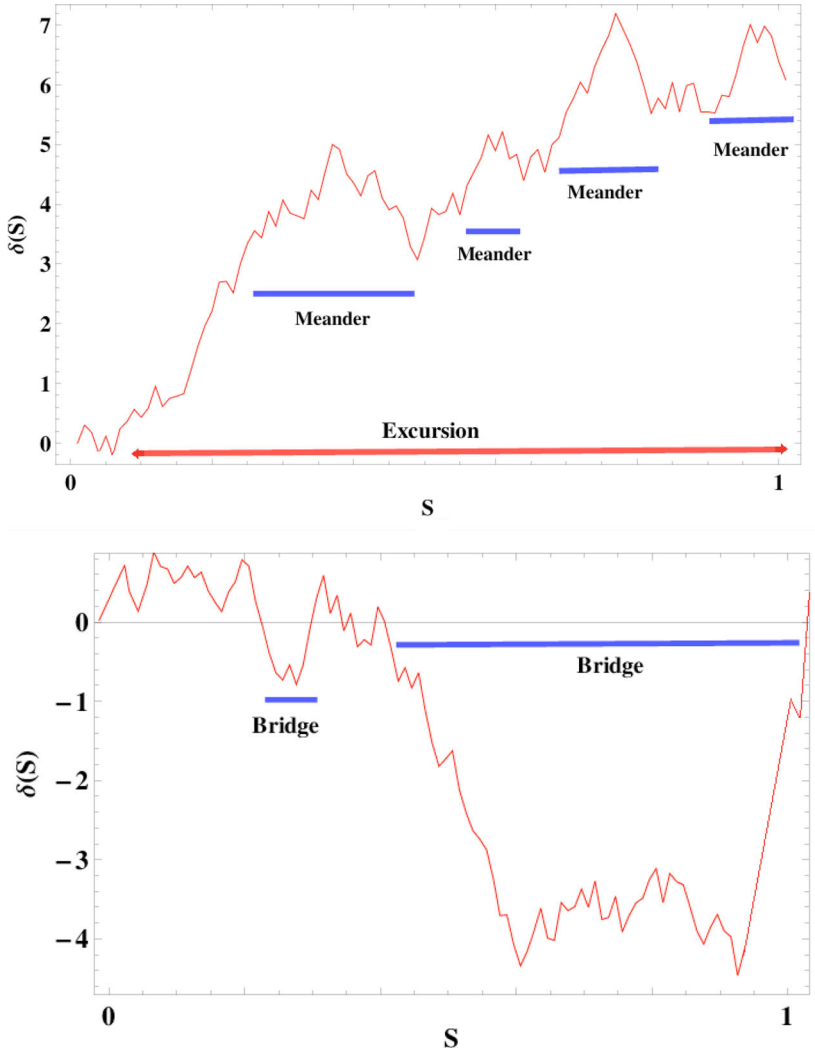


**Figure 3.** Three characteristics of the Brownian random walk: excursion, meander (upper) and bridge (lower). (Upper) The excursion characteristic of Brownian motion is a positive definite random walk. It is shown in red and it increases in each increment $\delta(S_1) < \delta(S_1 - S_2)$. Meander is always a positive definite local maximum in the positive definite excursion. However a Brownian bridge has negative values ($\delta(S) < 0$) for positive definite steps ($S > 0$). (Lower) Brownian bridges are defined as minima in a Brownian random walk. Note that the excursion characteristic of random walks can be described as a positive definite bridge.

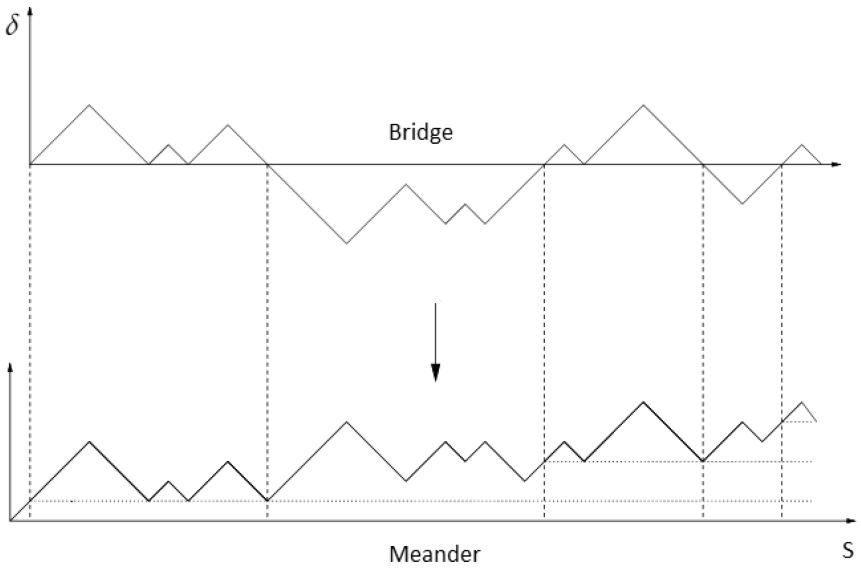


**Figure 4.** Method of transforming a bridge to a meander. There is bijection (one to one correspondence) between the negative valued walk (bridge) and the positive valued local maxima (meander) characteristics of Brownian random walks. To obtain a positive valued meander/excursion of certain length from a bridge, one needs to replace each negative excursion (barrier) of the bridge by its symmetric positive excursion. Then, the last negative step of this symmetric positive excursion should be replaced by a positive step. The final step is to add the first positive step to the whole path (Marchal 2003).

(iii) A Brownian meander is defined as a cumulative random walk of density contrast, $\delta(S)$ which has length $<S$ and $\delta(S)$ is conditioned to stay positive in the interval (Fig. 3). In the EPS formalism, meander represents local maxima with positive barriers in a Brownian excursion, indicating collapse regions.

In the context of the EPS/excursion set theory, the cloud in cloud problem can be related to the excursion characteristic of the Brownian random walk, while the void in cloud problem admits the combination of two characteristics of the Brownian random walk, that of a meander with a positive barrier, indicating a collapse region, and a bridge with a negative barrier, indicating a merging region. These definitions of the conditioned Brownian motions have been rigorous in many ways (Vervaat 1979; Fitzsimmons, Pitman & Yor 1993; Pitman 1999; Marchal 2003). There is a simple and an effective method developed by Marchal (2003) that allows one to transform a negative definite bridge into a positive definite meander/excursion. Recall that there is a bijection between the bridge and the meander. To construct a meander/excursion of length $2S + 1$ from a bridge of length $2S$, one must replace each negative excursion of the bridge by its symmetric positive excursion and replace the last negative step of this symmetric positive excursion by a positive step. Finally a first positive step must be added to the whole path (barrier uplifting) (Fig. 4).

### 3.3 Void in cloud problem: From bridge to excursion

Following the definitions of the Brownian characteristics of the random walk and the method to obtain a positive definite excursion, here a simple treatment to the void in cloud random walk is defined and discussed to describe it in terms of the EPS formalism.

As mentioned before, the void in cloud random walk has one negative signed deep bridge on large volume scales (see panel *A* in Fig. 5) with a negative barrier ($\delta_v$) and one positive signed meander (or excursion) on the small mass scales with a positive barrier $\delta_c$. Note that as of now, the volume distribution function is adopted in terms of volume scale $S(V)$ to describe volume evolution in the context of void hierarchy. The distribution of the void population is given by Sheth & van de Weygaert (2004) as follows:

$$f_v\,\mathrm{d}S \approx \frac{1}{\sqrt{2\pi}}\frac{\delta_v}{S^{2/3}}\exp\left[-\frac{\delta_v^2}{2S}\right]\exp\left[-\frac{\delta_v}{\delta_c}\frac{S}{4\delta_v^2\left(\frac{\delta_c}{\delta_v}+1\right)^2}-2\frac{S^2}{\delta_v^4\left(\frac{\delta_c}{\delta_v}+1\right)^4}\right]\mathrm{d}S. \tag{12}$$

Here, this distribution function is taken with a partially negative random walk and makes this a complete positive excursion without changing its probability distribution. To do this by following the remark of Theorem, each excursion of the whole walk is replaced by their symmetric excursion. This happens by taking the mirror of the distribution around the $x$-axis ($S$) (see *B* in Fig. 5). However, here there is still a negative bridge crossing the negative collapse barrier which is not allowed in the EPS formalism. To solve this problem, the barriers are shifted up by $2\delta_c$ with an accompanying shift in the probability distribution (see *C–D* in Fig. 5). Then, none of the barriers have a negative value and the resulting distribution function is given by

$$f_v\,\mathrm{d}S \approx \frac{1}{\sqrt{2\pi}}\frac{|\tilde{\delta}_v|}{S^{2/3}}\exp\left[-\frac{\tilde{\delta}_v^2}{2S}\right]\exp\left[-\frac{1}{\tilde{\gamma}}\frac{1}{(\tilde{\gamma}+1)^2}\frac{S}{4\tilde{\delta}_v^2}-2\frac{S^2}{\tilde{\delta}_v^4(\tilde{\gamma}+1)^4}\right]\mathrm{d}S, \tag{13}$$

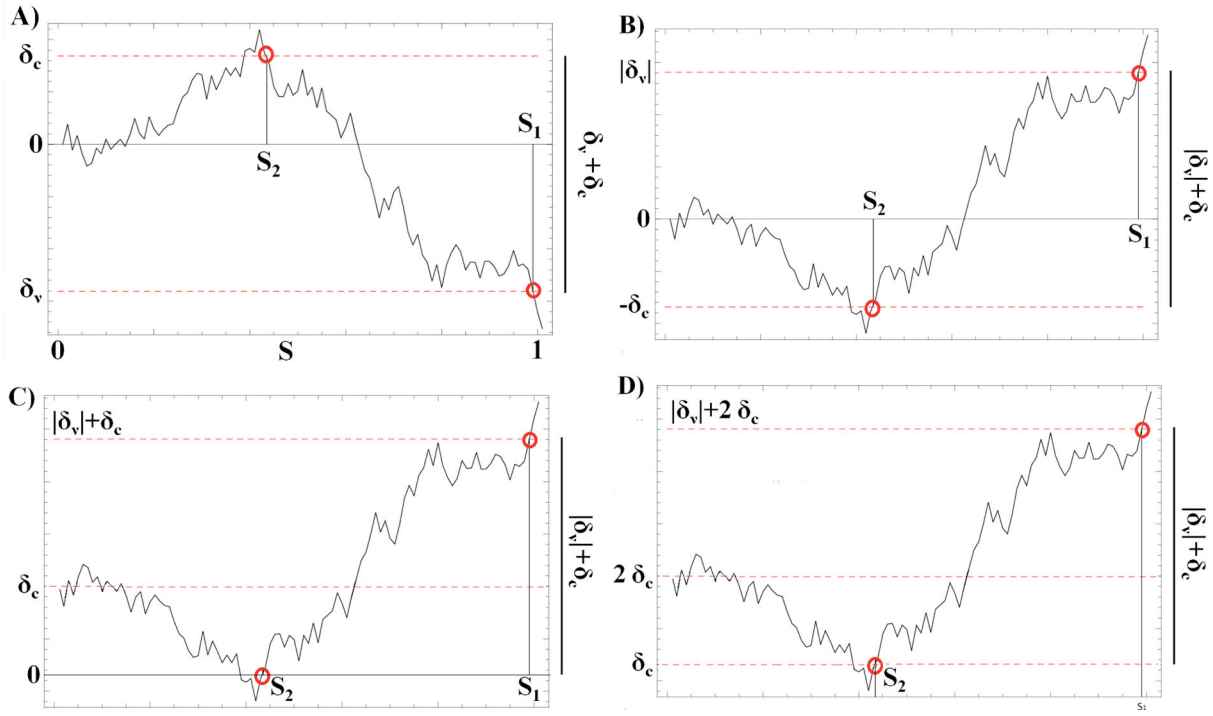


**Figure 5.** Steps of constructing excursion with positive barriers from the void in cloud random walk with a negative definite bridge characteristic.

where a new barrier $\tilde{\delta}_v$ is defined. This new barrier is given by

$$\tilde{\delta}_v \equiv |\delta_v| + 2\delta_c, \tag{14}$$

while the new barrier height ratio $\tilde{\gamma}$ is defined as,

$$\tilde{\gamma} \equiv \frac{\delta_c}{|\tilde{\delta}_v|}. \tag{15}$$

Hereafter the new barrier ratio is called the parametrized barrier ratio. Therefore, a positive excursion random walk (Brownian random walk) of the void evolution is obtained. This allows us to form the void mass/volume scale function that mimics the excursion set formalism of haloes. By applying this method which constructs an excursion set from a negative defined bridge.

(i) The distance between the barriers is not changed (see Fig. 4). In addition to this, the scales where the random walk meets the barriers is not changed either. The only change is that the distribution with negative barriers becomes a completely positive Brownian random walk, like the excursion set formalism (see Bond et al. 1991).

(ii) Since the distance of the barriers and the volume scales where the trajectories make their first upcrossing are not changed by the barrier shifting up process, the probability distribution does not change. This allows us to use the two-barrier fraction function given by Sheth & van de Weygaert (2004).

Now the questions are: how can we obtain a merger tree algorithm from this distribution, and what is the physical interpretation of this distribution from the void perspective?

Fig. 6 shows the random walk of the void in cloud which is converted into a positive excursion set by following the method, that is introduced above. This method has a key role since it allows one to treat the random walk of the void in cloud as a cloud in cloud random walk. As a result, in Fig. 6, a given trajectory $\delta(S)$ describes the merging history for a given void which starts its evolution with volume scale $S_1$ at barrier $\tilde{\delta}_v$, and later it will merge into other voids with larger volume at smaller barrier values $< \tilde{\delta}_v$ and eventually will collapse at barrier $\delta_c$ corresponding to volume scale $S_2$. Note that in Fig. 6, the random walk makes horizontal jumps when $S$ decreases. These jumps correspond to sudden jumps in the volume of the void. The small steps in between two barriers correspond to adding only a small amount of volume to the void. These events are called void absorption events, since bigger voids absorb small ones. Note that after several merges with other voids, the void will reach the end of its lifetime when its random walk crosses the collapse barrier $\delta_c$. This means that the collapse barrier represents the end of void merging events.

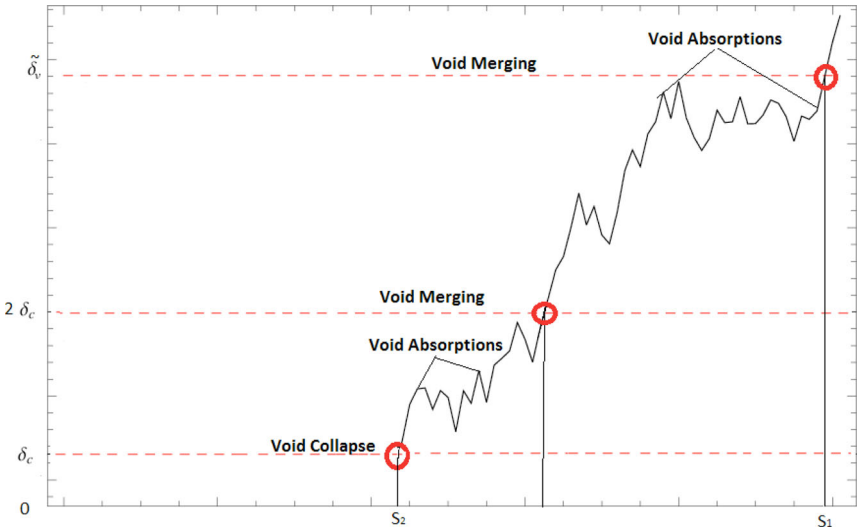


**Figure 6.** Excursion set interpretation of the void in cloud process. A given trajectory $\delta(S)$ describes the history of an embedded/minor void that starts merging with volume scale $S_1 = S(V_1)$ at shell crossing/merging barrier $\tilde{\delta}_v$ and later on collapses at barrier $\delta_c$ corresponding volume scale $S_2$.

### 3.4 Redshift and size constraints on voids

The parameters $\gamma$ and $\tilde{\gamma}$ are defined as the ratio of the collapse and underdense barriers of the random walks,

$$\gamma = \frac{\delta_c}{|\delta_v|} \quad \text{and} \quad \tilde{\gamma} \equiv \frac{\delta_c}{\tilde{\delta}_v} = \frac{\delta_c}{|\delta_v| + 2\delta_c}. \tag{16}$$

The relation between the barrier ratios is given by

$$\tilde{\gamma} = \frac{\gamma}{2\gamma + 1}. \tag{17}$$

The backbone of the constraints of the extended void merging tree is formed by the fact that the earliest merging barrier $\delta_v$ must be bigger than the $2\delta_c$ in order to obtain a merging event and at the end of the excursion process the walk will cross the collapse barrier,

$$\tilde{\delta}_v = |\delta_v| + 2\delta_c \quad \text{and} \quad \tilde{\delta}_v > |\delta_v| > 2\delta_c. \tag{18}$$

Note that $\tilde{\delta}_v$ stands for the first merging event with the biggest volume scale $S(V_1)$ indicating a void with smallest volume in the EPS formalism. Taking into account $|\delta_v| > 2\delta_c$, it is possible to obtain relations between merging $z_v$ and collapse $z_c$ redshifts,

$$z_v > 2\frac{\delta_{c0}}{\delta_{v0}}(1 + z_c) - 1. \tag{19}$$

In this study, in all calculations for plots, the collapse redshift is chosen as present-day redshift $z_c = 0$. As a result, for this collapse redshift $z_c = 0$, a lower limit of merging redshift is obtained as $z_v > 0.2$. The condition (18) puts a constraint on the barrier ratio $\gamma$ as $\gamma < 0.5$.

Another constraint on the barrier ratio $\gamma$ resulting from the merging redshift comes from the theoretical study of Sheth & van de Weygaert (2004). In their study, Sheth & van de Weygaert (2004) point out that two barrier mass fraction function (7) is accurate for values of $\gamma \geq 1/4$. This allows us to obtain an upper merging redshift value as $z_v \leq 1.4$. Hence, the constraints on the barrier ratio and the merging redshift are given as

$$0.25 \leq \gamma < 0.5 \quad \text{and} \quad 0.2 < z_v \leq 1.4 \ \text{ at } \ z_c = 0. \tag{20}$$

One may show that,

$$\tilde{\gamma} = \frac{\gamma}{2}, \tag{21}$$

by using the relation between $\gamma$ and $\tilde{\gamma}$ (17) in the limit of $|\delta_v|$ tends to $2\delta_c$ ($\gamma \to 0.5$). As a consequence of this relation, the interval of the parametrized barrier height ratio $\tilde{\gamma}$ can be obtained as

$$0.125 \leq \tilde{\gamma} < 0.25. \tag{22}$$

In addition to this, from the relations (16) and (17), it is obtained that when the collapse barrier is moved towards infinity $\delta_c \to \infty$, $\gamma$ tends to infinity. As a result, from the relation (11), the new barrier ratio becomes $\tilde{\gamma} \geq 0.5$. Therefore, the distribution turns into the one-barrier distribution of the void in void problem in Fig. 2. Based on this, two different void behaviours are modelled by the following constraints.

(i) Void collapse: contribution of the small voids into the distribution is dominant: 'Voids are squeezed',

$$0.125 \leq \tilde{\gamma} < 0.25 \quad \text{and} \quad 0.2 < z_v \leq 1.4 \ \text{ for } z_c = 0. \tag{23}$$

(ii) Void merging: when the ratio of collapse and merging barriers is high, $\delta_c \gg |\delta_v|$, the new barrier height parameter becomes $\tilde{\gamma} \gg 0.5$. The two-barrier excursion set theory is reduced to the one-barrier void in void problem. Therefore, voids do not vanish due to collapsed regions where they are embedded and their evolution is dominated only by merging events (Russell 2013).

An important result on the void volume scale is given by Sheth & van de Weygaert (2004). This criterion is based on the statement that there are no large-scale voids embedded in large-scale haloes, on the scales where,

$$\sigma \ll (\delta_c + |\delta_v|)\,, \tag{24}$$

and the collapse barrier $\delta_c$ does not have any effect on the void population. If this statement is rearranged in terms of the void size, a size criterion on void sizes that do not feel the environmental effects can be obtained as

$$R \gg \; R_*\,(\gamma+1)^{-\frac{2}{n+3}}\,, \qquad \gamma > 0.5, \tag{25}$$

where the characteristic radius $R_*$ is chosen as $R_* = 8\,h^{-1}$ Mpc. This size criterion leads to a rough classification between void sizes. Some voids are embedded in the overdense regions and eventually collapse (with $0.25 \leq \gamma < 0.5$ or $0.125 \leq \tilde{\gamma} < 0.25$) while other voids that satisfy this size criterion and expand, merge continuously ($\gamma > 0.5$ or $\tilde{\gamma} > 0.25$). In the limit of the above redshift and the size criterion, their EPS formalism should satisfy the one-barrier EPS formalism of the growing voids (Russell 2013). In a way, the last case is just a theoretical statement since it is not possible for some voids to merge and expand forever.

In the following section, the evolutionary paths of these two void groups are investigated in terms of the EPS formalism by adapting the LC93 merging tree algorithm.

## 4 MERGING TREE ALGORITHM OF GROWING AND EMBEDDED/MINOR VOIDS

Here, the aim is to determine the merger probability per unit time for a void of a given volume and time. Therefore, the subset of trajectories is considered, depicted in Fig. 7. These trajectories make their first upcrossing of a barrier $\delta_c$ at $S_2$ and then continue until they eventually cross a second barrier of height $\tilde{\delta}_v$ at various scales $S_1 > S_2$.

From the point of merging history of voids, these trajectories represent voids which at the time corresponding to $\tilde{\delta}_v$ have relatively large volume scales $S_1$s. Later on, these trajectories cross the collapse barrier $\delta_c$ where voids die after several times merging. Note that in between the first merging barrier and the last collapse barrier, many merging barriers can be replaced as long as the last barrier is the collapse one, $\delta_c$. The scale fraction function derived in equation (13) is

$$f_v\,\mathrm{d}S \approx \frac{1}{\sqrt{2\pi}}\frac{\tilde{\delta}_v}{S^{2/3}}\exp\!\left[-\frac{\tilde{\delta}_v^2}{2S}\right]\exp\left[-\frac{1}{\tilde{\gamma}}\frac{1}{(\tilde{\gamma}+1)^2}\frac{S}{4\tilde{\delta}_v^2} - 2\frac{S^2}{\tilde{\delta}_v^4\,(\tilde{\gamma}+1)^4}\right]\mathrm{d}S.$$

The conditional probability $f_{S_1}(S_1, \tilde{\delta}_v|S_2, \delta_c)\,\mathrm{d}S_1$ in which one of these trajectories makes its first upcrossing at $\tilde{\delta}_v$ in the interval $S_1 + \mathrm{d}S_1$ can be obtained directly from equation (13) but with a difference that the source of the trajectories moved from the origin to the point $(S_2, \delta_c)$ (by following the algorithm derived by LC93). Then, the conditional probability density of a void whose trajectory is in the interval $S_1 + \mathrm{d}S_1$ making its first up crossing at $\tilde{\delta}_v$ which collapses at the point $(S_2, \delta_c)$ is

$$f_{S_1}(S_1, \tilde{\delta}_v|S_2, \delta_c)\,\mathrm{d}S_1 = \frac{1}{\sqrt{2\pi}}\frac{\tilde{\delta}_v - \delta_c}{(S_1 - S_2)^{3/2}}\exp\left(\frac{-\left(\tilde{\delta}_v - \delta_c\right)^2}{2\,(S_1 - S_2)}\right)\exp\left(-\frac{1}{4}\frac{1}{\tilde{\gamma}}\frac{1}{(1+\tilde{\gamma})^2}\frac{S_1 - S_2}{\left(\tilde{\delta}_v - \delta_c\right)^2}\right)\exp\left(-2\frac{1}{(1+\tilde{\gamma})^4}\frac{(S_1 - S_2)^2}{\left(\tilde{\delta}_v - \delta_c\right)^4}\right)\mathrm{d}S_1. \tag{26}$$

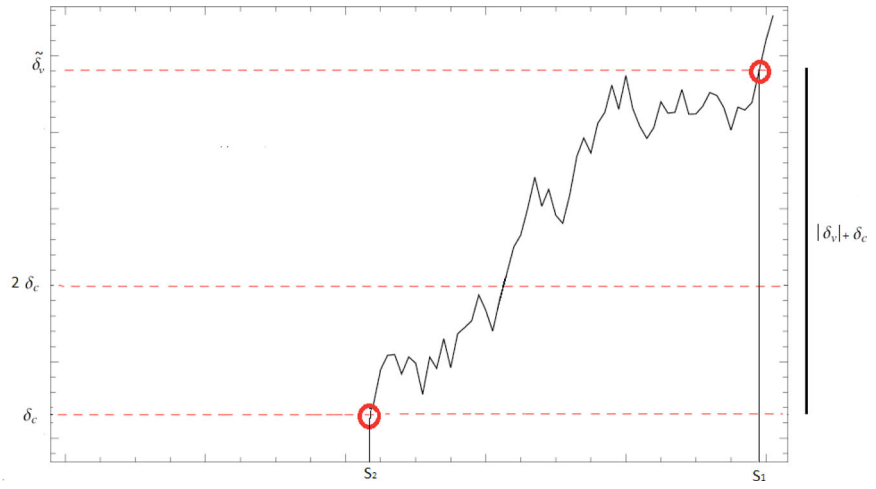


**Figure 7.** Subset of trajectories making their first upcrossing of a barrier $\delta_c$ at $S_2$ and then continue until crossing a second barrier $\tilde{\delta}_v$ at various scales $S_1 > S_2$. These trajectories represent voids which at the time corresponding to $\tilde{\delta}_v$ have volumes corresponding to $S_1(V)$, which by the later time correspond to the scale $\delta_c$ at volume scale $S_2(V)$ where they will vanish due to collapse.

Here, $\tilde{\delta}_v > \delta_c$ ($\approx z_v > z_c$) and the volume scale is $S_1 > S_2$. Note that high volume scale indicates small-size radius. Hence, the void size fraction derived from equation (26) for the self-similar models becomes

$$f_{R_1}(R_1, \tilde{\delta}_v | R_2, \delta_c)\, \mathrm{d}R_1 = \frac{3\alpha}{\sqrt{2\pi}} \frac{\tilde{\delta}_v^2}{R_*} \left(\frac{R_1}{R_*}\right)^{-3\alpha-1} \frac{\tilde{\delta}_v - \delta_c}{\left(\tilde{\delta}_v^2 \left(\frac{R_1}{R_*}\right)^{-3\alpha} - \delta_c^2 \left(\frac{R_2}{R_*}\right)^{-3\alpha}\right)^{3/2}} \exp\left(\frac{-\left(\tilde{\delta}_v - \delta_c\right)^2}{2\left(\tilde{\delta}_v^2 \left(\frac{R_1}{R_*}\right)^{-3\alpha} - \delta_c^2 \left(\frac{R_2}{R_*}\right)^{-3\alpha}\right)}\right)$$

$$\times \exp\left(-\frac{1}{4}\frac{1}{\tilde{\gamma}}\frac{1}{(1+\tilde{\gamma})^2} \frac{\tilde{\delta}_v^2 \left(\frac{R_1}{R_*}\right)^{-3\alpha} - \delta_c^2 \left(\frac{R_2}{R_*}\right)^{-3\alpha}}{\left(\tilde{\delta}_v - \delta_c\right)^2}\right) \exp\left(-2\frac{1}{(1+\tilde{\gamma})^4} \frac{\left(\tilde{\delta}_v^2 \left(\frac{R_1}{R_*}\right)^{-3\alpha} - \delta_c^2 \left(\frac{R_2}{R_*}\right)^{-3\alpha}\right)^2}{\left(\tilde{\delta}_v - \delta_c\right)^4}\right) \mathrm{d}R_1. \quad (27)$$

Depending on the value of the barrier ratio, equation (27) displays the size distribution of the embedded voids in one formula for the self-similar models. Fig. 8 shows embedded void size distributions for self-similar ($n = 0, -1, -1.5, -2$), respectively, at given redshift $z_v$ values satisfying the constraint equalities (23) at collapse redshift $z_c = 0$. Note that, in all models, the collapse redshift is chosen as $z_c = 0$ when minor voids collapse and vanish after merging at a given redshift $z_v$. In Fig. 8, the peak of a size distribution at a given redshift indicates a specific size. Embedded/minor voids with this size value dominate the distribution at a given redshift. In all self-similar models, peaks of the size distributions slightly move towards smaller sizes with increasing redshift $z_v$. This result may show that small size minor voids are numerous and they fill the Universe at high redshifts. This is what it is expected from the bottom-up hierarchical scenarios that small-size voids merge together and construct larger size voids. In addition, in the self-similar models, the peaks of the size distribution decrease with decreasing spectral index while the size range of minor voids increases drastically when the spectral index decreases. For example, the size distribution $f_{R1}$ in the model with spectral index $n = -2$ at redshift $z = 0.3$ shows $6 - 166\ h^{-1}$ Mpc void size range while one with spectral index $n = 0$ at the same redshift has $7{-}25\ h^{-1}$ Mpc size range. Note that decreasing spectral index corresponds to an increase in hierarchical clustering. Therefore, one may say that the probability of detecting an embedded void with size $50\ h^{-1}$ Mpc is most likely in the model with spectral index $n = -2$ than in the self-similar model with index $n = 0$. On the other hand, in all models, size distribution shows two cut-offs corresponding to the smallest and the largest size values at a given redshift $z_v$. As is seen in Fig. 8, these cut-off values have the smallest probability values. While the small cut-off becomes smaller, the big cut-off moves towards higher values by decreasing spectral index for a

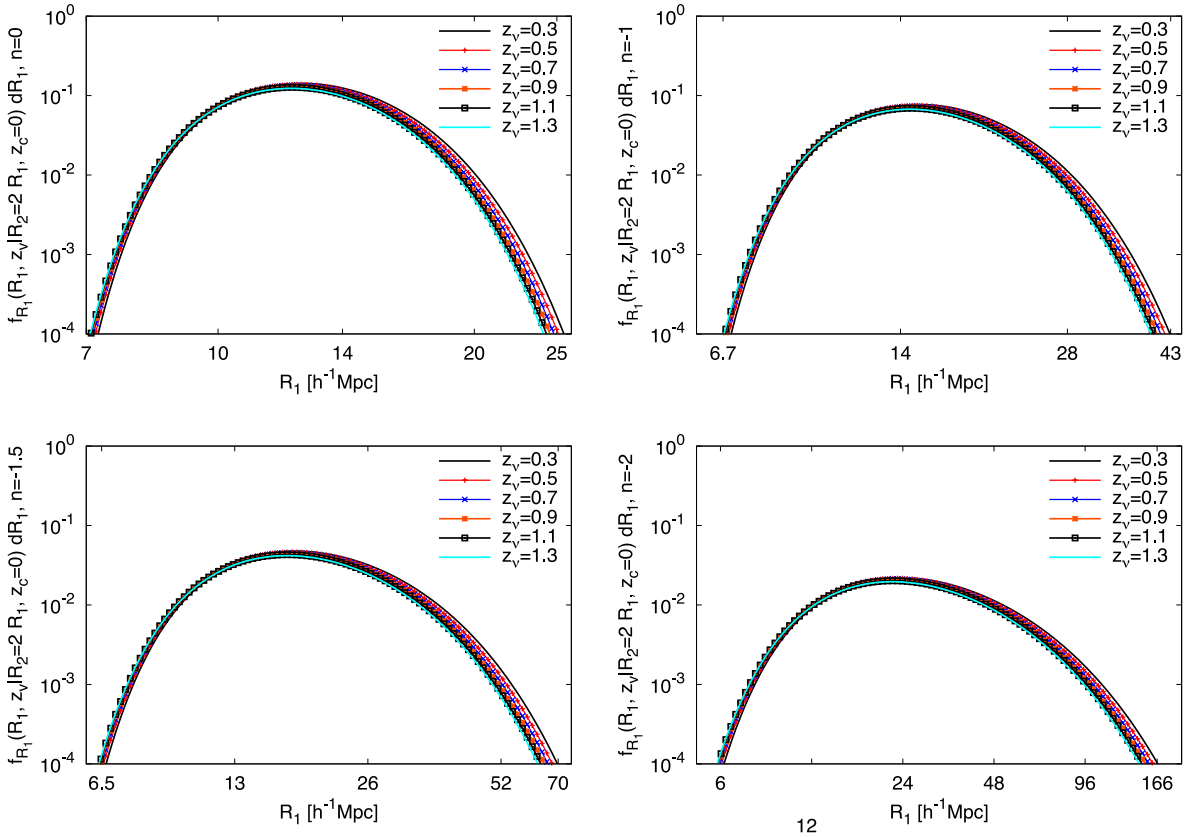


**Figure 8.** Size distribution of voids embedded in overdense regions at given redshift $z_v$ in terms of $R_1$ [$h^{-1}$ Mpc] for the self-similar $n = 0, -1, -1.5, -2$ at redshifts $z_v = 0.3, 0.5, 0.7, 0.9, 1.1, 1.3$. Later on voids with size $R_1$ at redshift $z_v$ will double their size, $R_2 = 2R_1$ at collapse redshift $z_c = 0$ when they will vanish due to the presence of a collapse region.

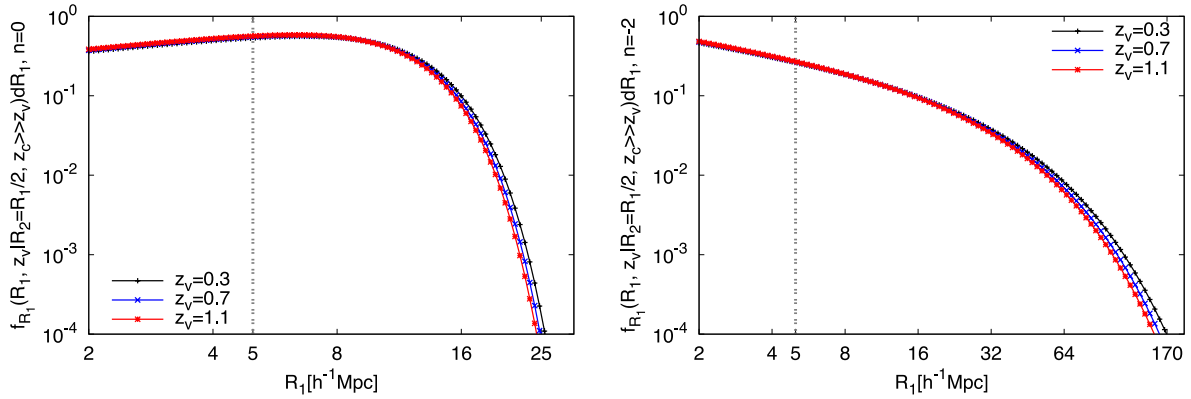


**Figure 9.** Size distributions of embedded growing voids. These voids are not affected by collapse regions at given redshifts $z_v = 0.3, 0.7, 1.1$ for self-similar models $n = 0, -2$. In the models, the collapse barrier is inserted at very high redshift satisfying $z_c \gg z_v$, corresponding to the relation $\delta_c \gg \delta_v$. The vertical line at size 5 $h^{-1}$ Mpc represents the limit of non-linearity corresponding to voids smaller than this size indicating non-linearity effects.

given redshift $z_v$. This behaviour indicates that the probability of seeing the largest and smallest size embedded voids at a given redshift and a given model is unlikely. In Fig. 9, the growing void distributions are plotted from minor void size distribution equation (27) by choosing $\delta_c \gg \delta_v$ (void in void limit). In this limit, embedded/minor voids are not affected by their surroundings. Therefore, they merge continuously. As is seen in Fig. 9, differing from the embedded/minor voids, the growing embedded void probability does not show the same feature as the minor void distribution. Instead, maxima in the growing embedded void distribution increase with decreasing spectral index (from $n = 0$ to $n = -2$) towards small-size voids. This behaviour is consistent with the one-barrier EPS formalism of growing voids constructed by Russell (2013). However, like the minor void case, the maxima in the size distribution increase with increasing redshift value. In Fig. 9, the vertical line at 5 $h^{-1}$ Mpc stands for the limit of non-linear effects. Both void populations with sizes smaller than 5 $h^{-1}$ Mpc are highly effected by non-linear effects. Therefore, they tend to have deformed or elliptical shapes. Note that in this study, the spherical void merging tree model is investigated. As a result, non-linear effects are neglected in the extended void merging algorithm when they are smaller than the 5 $h^{-1}$ Mpc limit. On the other hand, in Fig. 8, the size distribution of embedded voids in all self-similar models does not present void sizes smaller than this limit value. Therefore, the extended void size distribution based on the two-barrier EPS formalism is free of non-linear effects. To clarify the similarities and differences between minor and growing void size distributions that are derived from equation (27), in Fig. 10, the size distribution equation (27) is displayed for embedded/minor voids with the barrier ratio $\gamma = 0.3$ ($\tilde{\gamma} = 0.15$) (left) and growing voids with $\gamma \gg 0.5$ ($\tilde{\gamma} \gg 0.25$) (right) for self-similar with index $n = 0, -1, -1.5, -2$ models are presented. According to this, the size distribution equation (27) of embedded/minor and embedded/growing voids indicate a broad range in void sizes with decreasing spectral index. Generally speaking, the distribution of minor and growing voids decreases with decreasing spectral index. Embedded/minor void distributions show two cut-offs at very small and large sizes, while growing void population distributions indicate one cut-off at the largest sizes. In addition, in the growing void population, the smallest size voids show the highest distributions. Taking into account that decreasing spectral index indicates hierarchical clustering, obtaining larger size embedded voids in the self-similar models with smaller spectral index is expected. Therefore, even though very large and small embedded voids are possible to be seen in the embedded void population, they are rare compared to the embedded voids that form the peaks of the distributions. On the other hand, the growing void population retains numerous small voids while large voids are less numerous.

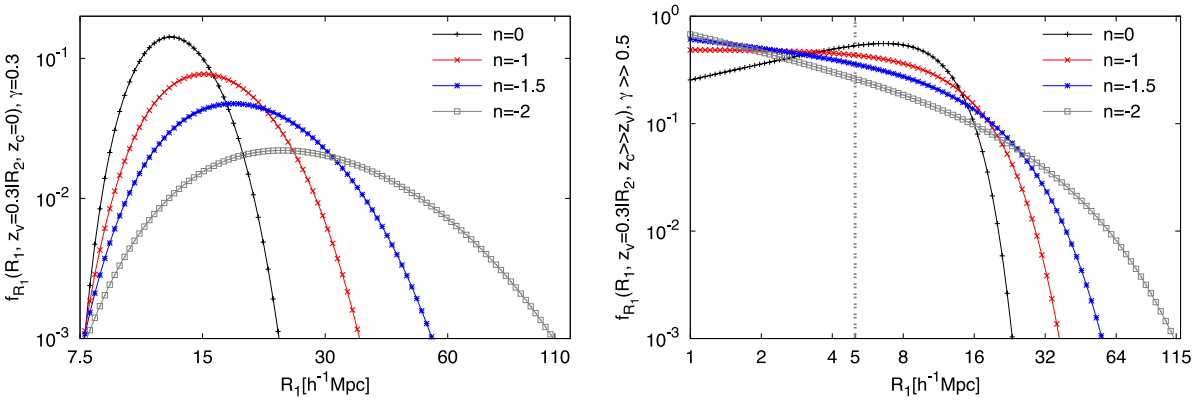


**Figure 10.** Size distribution of embedded/minor voids $\tilde{\gamma} = 0.15$ (or $\gamma = 0.3$) (left) and growing voids with the barrier ratio $\tilde{\gamma} \gg 0.25$ (right) from equation (27) in terms of self-similar with spectral index $n = 0, -1, -1.5, -2$ models. In all models merging redshift is chosen as $z_v = 0.3$ for minor voids while the collapse redshift is moved towards late redshift $z_c \gg z_v = 0.3$. The vertical line corresponds to 5 $h^{-1}$ Mpc size limit of non-linearity. Evolution of voids that are smaller than this size is formed by non-linearity effects.

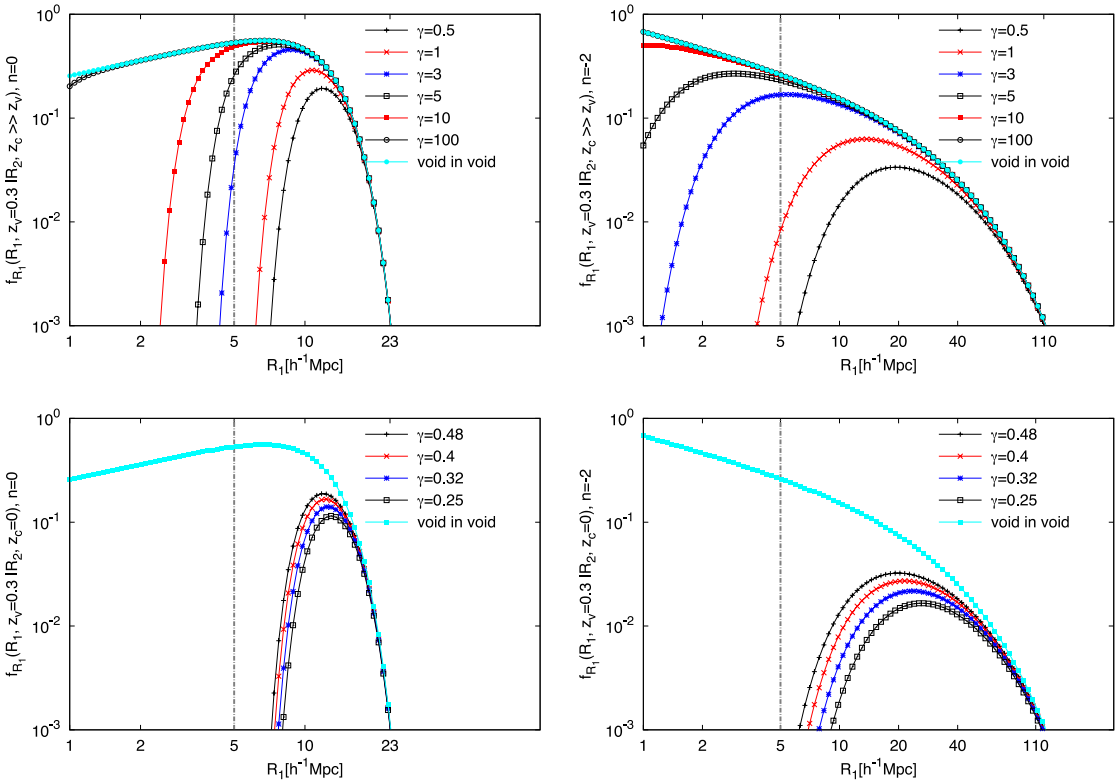


**Figure 11.** The barrier ratio dependence of the size distribution of growing (upper) and minor (lower) voids in the two-barrier EPS formalism for self-similar models with index $n = 0$ and $-2$. The two-barrier growing void size distribution is presented for the barrier ratio $\gamma \geq 0.5$ and then $z_c \gg z_v = 0.3$ while the barrier ratio dependence of the size distribution of minor voids is displayed by choosing $\gamma < 0.5$, $z_v = 0.3$ and $z_c = 0$.

As was pointed out before, the barrier height ratio has the key importance of defining hierarchical evolution of the void population by making a significant difference between minor and growing voids in the two-barrier excursion set. The barrier ratio dependence of the size probability distribution function (26) is shown in Fig. 11. The vertical line displayed in all panels is presented, with size $R_1 = 5\ h^{-1}$ Mpc. Voids with sizes smaller than this value may show non-linear effects. In this study, the non-linear effects are not considered. That is why voids with size $R_1 \geq 5\ h^{-1}$ Mpc are considered. In addition, in all panels, the void in void size distribution is inserted to show how the value of the barrier ratio affects the size distribution.

In Fig. 11, in the upper panels, growing void size distribution is presented for self-similar models with index $n = 0$ and $n = -2$. In both upper panels, the barrier ratio is chosen as $\gamma \geq 0.5$ and $z_c \gg z_v$. When the barrier height ratio increases, the conditional size distribution starts behaving like the size distribution of growing voids that are not affected by their environments as much as minor voids are. Particularly, when barrier ratio reaches large values $\gamma = 100$ indicating that collapse barrier is very large compared to merging barrier $\delta_c \gg \delta_v$ ($z_c \gg z_v$). As a result, placing merging barrier $\delta_c$ at very large redshift values, it is ensured that the distribution function becomes dominated by only merging events. Therefore, contribution of minor voids can be negligible in the size distribution. In the lower panels of Fig. 11, the minor void size distribution is displayed for the same models as in the upper panels. In the case of the minor void population size distribution, the barrier ratio is chosen as $\gamma < 0.5$ and $z_c = 0$ and $z_v = 0.3$. In minor and growing void size distributions, the peaks shift to small sizes when the barrier height ratio increases. While this shifting peak behaviour is not striking for minor voids with $\gamma < 0.5$, for growing voids with increasing barrier ratio $\gamma \geq 0.5$ the shifting behaviour becomes prominent. Also, peaks become flattened with increasing barrier height ratios. Therefore, there is a large diversity of sizes for growing voids. The peaks become flatter when the barrier ratio approaches the one-barrier $\tilde{\delta}_v$ ($\delta_c \gg \tilde{\delta}_v$). Therefore, the distribution turns into the 'void in void' one.

Another probability density function that can be derived from the random walks is the probability of a trajectory first up crossing $\delta_c$ then $\tilde{\delta}_v$ at $S_1$,

$$f_{S_2}(S_2, \delta_c | S_1, \tilde{\delta}_v)\, \mathrm{d}S_2 = \frac{1}{\sqrt{2\pi}} \frac{\delta_c \left(\tilde{\delta}_v - \delta_c\right)}{\tilde{\delta}_v} \left[\frac{S_1}{S_2\,(S_1 - S_2)}\right]^{3/2} \exp\left(-\frac{\left(\delta_c S_1 - \tilde{\delta}_v S_2\right)^2}{2 S_1 S_2\,(S_1 - S_2)}\right) \exp\left(-\frac{1}{4}\frac{1}{\tilde{\gamma}}\frac{1}{(1+\tilde{\gamma})^2}\left(\frac{S_1 - S_2}{\left(\tilde{\delta}_v - \delta_c\right)^2} + \frac{S_2}{\delta_c^2} - \frac{S_1}{\tilde{\delta}_v^2}\right)\right)$$
$$\times \exp\left(-2\frac{1}{(1+\tilde{\gamma})^4}\left(\frac{(S_1 - S_2)^2}{\left(\tilde{\delta}_v - \delta_c\right)^4} + \frac{S_2^2}{\delta_c^4} - \frac{S_1^2}{\tilde{\delta}_v^4}\right)\right) \mathrm{d}S_2. \tag{28}$$

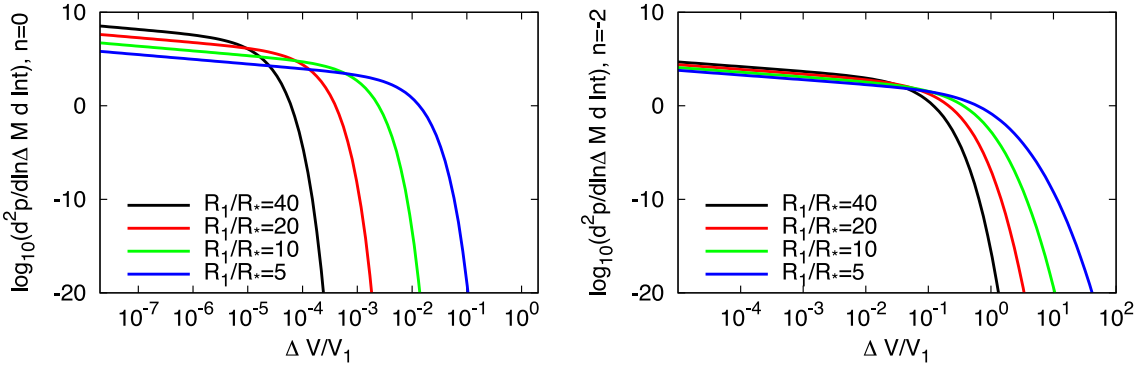


**Figure 12.** The merger rates of voids given by equation (31) for the self-similar models with the index $n = 0$ and $-2$ in terms of different radius ratios. They have the curve which is the highest on the left of each plot $R_1/R_* = 40$ and successive curves are $R_1/R_* = 20, 10, 5$.

This helps one to obtain merging rates of the two types of void processes. To do this, first the mean transition rate is derived by taking the limit $\delta_c \to \tilde{\delta}_v$,

$$\lim_{\delta_c \to \tilde{\delta}_v} \frac{\mathrm{d}^2 f_{S_2}(S_2, \delta_c | S_1, \tilde{\delta}_v) \mathrm{d}S_2}{\mathrm{d}S_2\, \mathrm{d}\delta} \equiv \lim_{\delta_c \to \tilde{\delta}_v} \frac{\mathrm{d}^2 p}{\mathrm{d}S_2 \mathrm{d}\delta}, \tag{29}$$

in which the functional $p$ is $p \equiv f_{S_2}(S_2, \delta_c | S_1, \tilde{\delta}_v)\, \mathrm{d}S_2$. This limit leads to a distribution function being obtained which changes in terms of barrier steps $\mathrm{d}\delta = \tilde{\delta}_v - \delta_c$ and as a result of the limit $\delta_c \to \tilde{\delta}_v$ corresponding to going back in time to obtain merging events, in equation (28) the last two exponentials indicating the tail of the faction disappear. Therefore, the distribution function is reduced to the following form:

$$\frac{\mathrm{d}^2 p}{\mathrm{d}S_2\, \mathrm{d}\tilde{\delta}_v}\left(S_1 \to S_2, \tilde{\delta}_v\right) = \frac{1}{\sqrt{2\pi}}\left[\frac{S_1}{S_2\,(S_1 - S_2)}\right]^{3/2} \exp\left[-\frac{\tilde{\delta}_v^2}{2}\frac{(S_1 - S_2)}{S_1 S_2}\right] \mathrm{d}S_2\, \mathrm{d}\delta. \tag{30}$$

Equation (30) is used by LC93 for overdense haloes in order to derive the merging rates of haloes and by Russell (2013) for gradually merging voids. Note that equation (30) is the same as the form of the one-barrier void merging distribution of Russell (2013). The only difference comes from the behaviours of the barriers; while one of the barriers is the collapse barrier $\delta_c$ instead of a second void merging barrier $\tilde{\delta}_{v_2}$. Equation (30) also can be interpreted as one or more merging void event(s) depending on expansion/underdense $\tilde{\delta}_v$ and collapse/overdense $\delta_c$ barriers. While any finite interval of $\Delta\delta = \tilde{\delta}_v - \delta_c$ at $\Delta S$ shows the cumulative effect of more than one merger, an infinitesimal interval $\mathrm{d}\delta$ at $\mathrm{d}S$ indicates a single void merger event. Hence, equation (30) represents the probability of a void with volume scale $S_1$ merging at later times with another void of volume $\Delta V = V_2 - V_1$. Thus, the rate of merging, divided by the volume $\Delta V$ of the void that it is being merged with, is,

$$\frac{\mathrm{d}^2 p}{\mathrm{d}\ln \Delta V \mathrm{d}\ln t}(V_1 \to V_2, |t) = \sqrt{\frac{2}{\pi}}\frac{\Delta V}{V_2}\frac{\tilde{\delta}_v(t)}{\sqrt{S_2}}\left|\frac{\mathrm{d}\ln\sqrt{S_2}}{\mathrm{d}\ln V_2}\right|\left|\frac{\mathrm{d}\ln\tilde{\delta}_v}{\mathrm{d}\ln t}\right|\frac{1}{(1 - S_2/S_1)^{3/2}}\exp\left[-\frac{\tilde{\delta}_v^2}{2}\left(\frac{1}{S_2} - \frac{1}{S_1}\right)\right]. \tag{31}$$

The merger rates of embedded/minor and growing voids are formulated by the same equation. Consequently, their merging rates show the same behaviour. Fig. 12 presents merger rates of embedded/minor voids of a given size in terms of self-similar models. According to this, in Fig. 12 the merger rates of the self-similar models decrease with increasing spectral index. This behaviour is less prominent in voids with smaller size ratios $R/R_* \leq 10\,h^{-1}$ Mpc than their large-size counterparts $R/R_* > 10\,h^{-1}$ Mpc. Due to this result, large-size voids contribute to the merging events more than smaller size voids.

## 5 TIMESCALES IN THE MERGING TREE ALGORITHM

In the following sections, survival and formation times of the two-barrier void hierarchy are defined and formulated. Recall that here the linear over and underdensities are used as time parameters following LC93. This is only allowed in the EdS Universe since linearly extrapolated densities are constant and only time dependency comes from the linear growth factor $\Upsilon$.

### 5.1 Void collapse and failure times

As is shown in the previous section, the merging rates of embedded voids have the same merging features as growing voids. The question is: What is the main distinction of these populations if it is not their merging character? The answer is their survival probabilities which form a separation between the two groups. Due to their environmental characteristics, it is expected that their survival times should be different since one of the groups vanishes under its gravitational collapse and the other one merges gradually. However in reality, before they collapse, we cannot really distinguish between them.

By following the definition of the survival time of growing voids by Russell (2013), the void survival time is defined as the time $\delta_{\rm surv}$ when the volume gets doubled $2V$ due to merging. The survival probability function of a void succeeding to merge and double in size, is

given by

$$\underbrace{P(S > S_2, \delta_{v_2}|S_1, \delta_{v_1})}_{\text{probability of survival beyond } S_2} = 1 - \underbrace{P(S < S_2, \delta_{v_2}|S_1, \delta_{v_1})}_{\text{probability of a void failing before reaching } S_2}, \tag{32}$$

where the survival probability distribution $P(S > S_2, \delta_{v_2}|S_1, \delta_{v_1})$ varies between one and zero indicating survival and death processes. Although the same survival profile from both void populations is expected, the survival probability of the void population shows two different behaviours based on their survival size distribution, which is strongly related with their environmental properties. For example for embedded voids, it is expected that the probability of a void failing before reaching its double size should be related with the collapse event due to the presence of overdense regions in their environment. The effect of gravitational collapse of overdense regions slows down the void merging process and forces the void evolution to stop, or may even make them vanish. Here, these two different behaviours are obtained depending on the barrier ratios. As is mentioned before, the value of the barrier ratio is the key element of the two-barrier excursion set since it makes a distinction between merging and collapsing behaviours of the void population. In this sense, the barrier ratio $\tilde{\gamma}$ or $\gamma$ can be considered as an environmental indicator. When the ratio of the two barriers is higher than the value $\delta_c/\tilde{\delta}_v \geq 0.5$, the collapse barrier becomes larger $\delta_c \gg \tilde{\delta}_v$. As is known, this is the indication of gradual merging events (Sheth & van de Weygaert 2004; Russell 2013). In the limit of $\tilde{\gamma} < 0.25$ (or $\gamma < 0.5$), the two barriers get closer. Due to the collapse barrier, the merging event cannot be a continuous event. By taking into account these two possibilities, here two survival probability functions of voids are obtained, whereby they merge gradually and first they merge and later on collapse.

*Survival probability of growing voids.* The survival probability of voids that merge at the volume scale $S_2$ and survive and continue merging after this certain scale, is defined as the probability of a void making its transition from $S < S_2$ to $S > S_2$ at barrier $\delta > \delta_{v_2}$ and its explicit form given by Russell (2013),

$$\begin{aligned} P(S > S_2, \delta_{v_2}|S_1, \delta_{v_1}) &= 1 - \int_0^{S_2} f_{S_2}\left(S_2', \delta_{v_2}|S_1, \delta_{v_1}\right) \mathrm{d}S_2' \\ &= \sqrt{\frac{2}{\pi}}\delta_{v_1} - \delta_{v_2}\left|\frac{\delta_{v_2}}{\delta_{v_1}}\right| \left[\sqrt{\frac{S_2}{S_1\left(S_1 - S_2\right)}} \mathrm{e}^{-\frac{\delta_{v_1}^2}{2}\left(\frac{1}{S_1} - \frac{1}{S_2}\right)} + \sqrt{\frac{\pi}{2}}\frac{1}{\delta_{v_1}}\left(\frac{\delta_{v_1}^2}{S_1} - 1\right) \times \mathrm{erf}\sqrt{\frac{\delta_{v_1}^2}{2}\left(\frac{1}{S_1} - \frac{1}{S_2}\right)}\right]. \end{aligned} \tag{33}$$

Since the collapse barrier tends to be infinite, this implies the collapse event occurred in the past. Therefore, minor void contribution to the survival probability becomes negligible. As a result, voids continue their merging behaviour gradually. Therefore, the two-barrier problem is reduced to a one-barrier problem and void evolution can be modelled with only one type of barrier $\delta_v$. It is also possible to derive the distribution of times (Russell 2013),

$$\begin{aligned} F_{\delta_{v_2}} &= -\mathrm{d}\delta_{v_2}\left(\frac{\partial P(S > S_2, \delta_{v_2}|S_1, \delta_{v_1})}{\partial \delta_{v_2}}\right) = \mathrm{d}\delta_{v_2}\left(\frac{\partial P(S < S_2, \delta_{v_2}|S_1, \delta_{v_1})}{\partial \delta_{v_2}}\right) \\ &= \sqrt{\frac{2}{\pi}}\left|1 - 2\frac{\delta_{v_2}}{\delta_{v_1}}\right| \left[\sqrt{\frac{S_2}{S_1\left(S_1 - S_2\right)}} \mathrm{e}^{-\frac{\delta_{v_1}^2}{2}\left(\frac{1}{S_1} - \frac{1}{S_2}\right)} + \sqrt{\frac{\pi}{2}}\frac{1}{|\delta_{v_1}|}\left(\frac{\delta_{v_1}^2}{S_1} - 1\right) \mathrm{erf}\sqrt{\frac{|\delta_{v_1}^2|}{2}\left(\frac{1}{S_1} - \frac{1}{S_2}\right)}\right]. \end{aligned} \tag{34}$$

Russell (2013) defines the survival time distribution of a growing void population as the probability of a void with volume scale $S_1 = S(V_1)$ being incorporated into a system of volume larger than the corresponding scale $S_2 = S(V_2)$ during the time interval $\mathrm{d}\delta_{v_2}$ by adapting the survival times of dark matter haloes of LC93. As is pointed out in Russell (2013), the negative sign of the survival time distribution, equation (34), is known as the conditional failure rate or hazard function in statistical mathematics. Then equation (34) measures the failure rate of void radii that could not merge at a given redshift or measures the risk of voids not merging/growing for a given size with respect to a time interval.

*Collapse probability of embedded/minor voids.* The concept of survival probability of embedded/minor voids is slightly different than their growing counterparts. Unlike growing voids, embedded voids collapse at the volume scale $S_2$ instead of surviving. Therefore, the survival embedded void probability is named as the collapse probability, since it is the chance of an embedded void to collapsing. Then the collapse probability is defined as the probability of a void making its transition from $S < S_2$ to $S > S_2$ at barrier $\delta_c$ and vanishing at this collapse barrier $\delta_c$. Similarly to the survival probability of a growing void, the mathematical description of the collapse probability of an embedded/minor void is given by

$$\underbrace{P(S \geq S_2, \delta_c|S_1, \tilde{\delta}_v)}_{\text{probability of collapsing beyond } S_2} = 1 - \underbrace{P(S \leq S_2, \delta_c|S_1, \tilde{\delta}_v)}_{\text{probability of a void failing before reaching } S_2}. \tag{35}$$

Similar to the survival probability of growing void population, the collapse probability of the embedded voids $P(S \geq S_2, \delta_c|S_1, \tilde{\delta}_v)$ varies between one and zero, corresponding to success in collapse and failing. Hence, the collapse probability by using equations (35) and (13) is derived analytically as

$$P_{\mathrm{coll}}\left(S \geq S_2, \delta_c|S_1, \tilde{\delta}_v\right) = 1 - \int_0^{S_2} f_{S_2}\left(S_2', \delta_c|S_1, \tilde{\delta}_v\right) \mathrm{d}S_2' = 1 - \mathrm{e}^{-\frac{2}{3}\frac{S_1}{\delta_v^2} - y_n\frac{S_1^2}{\delta_v^4}} \mathrm{erf}\left(\frac{\delta_c}{\sqrt{2S_1}}\left(\frac{S_1 - 2S_2}{\sqrt{S_2\left(S_1 - S_2\right)}}\right)\right), \tag{36}$$

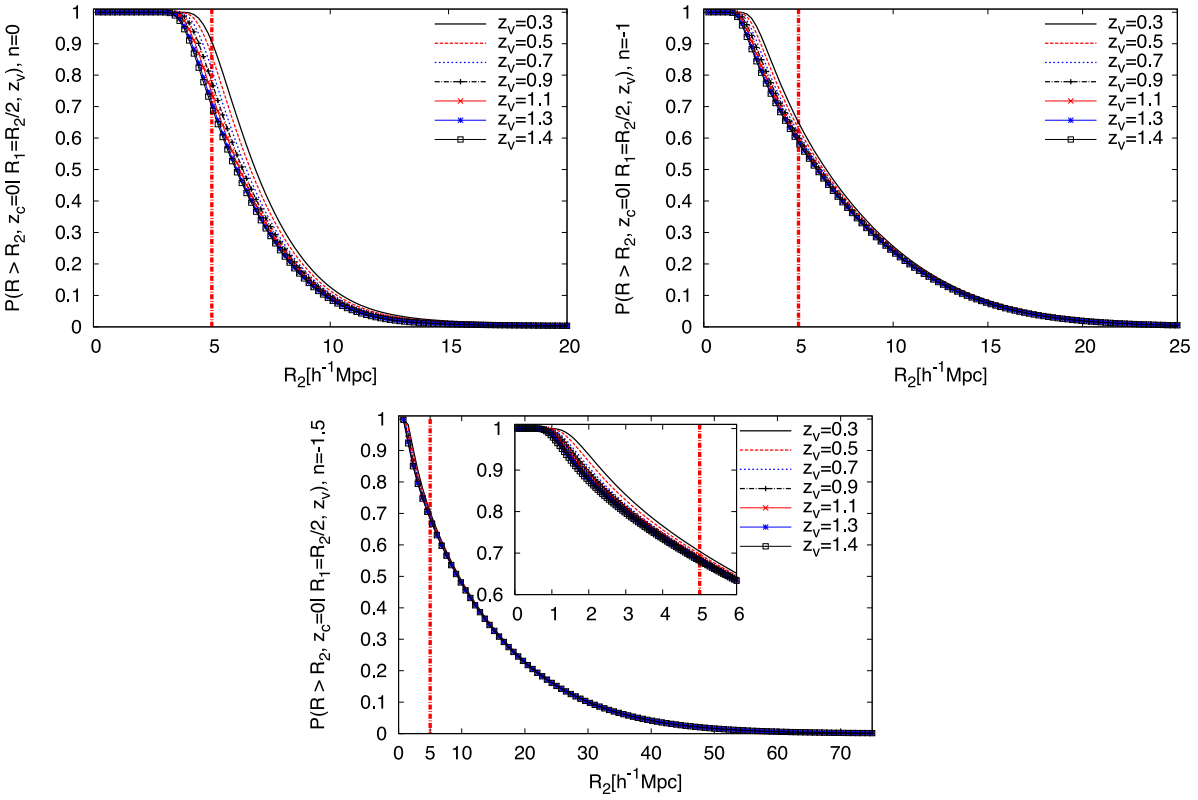


**Figure 13.** The collapse size distribution of embedded voids for self-similar models with index $n = 0, -1, -1.5$. In all models, the collapse probability of an embedded void is displayed in terms of radius $R_1$ at a given redshift $z_v$ which later on collapses at $z_c = 0$ when it doubles in size $R_2 = 2\,R_1$.

where $y_n$ (in which $n = 0, -1, -1.5, -2$) is a model-dependent numerical value that admits the following values for the self-similar models,

$$y_0 = 2.77, \qquad y_{-1} = 2.98, \qquad y_{-1.5} = 3.307, \qquad y_{-2} = 3.86. \tag{37}$$

Here, the spherical model is adopted which leads to the barrier ratio $\gamma = 0.5$ (Sheth & van de Weygaert 2004) and binary merging which gives the relation of scales depending on the self-similar model $S_2 \approx 2^{-\alpha} S_1$. The scales should be set as $S_1 = S(V)$, $S_2 = S(2V)$ due to the binary merging method. The dynamical variables of the hierarchical evolution are defined by the linear over and underdensities $\tilde{\delta}_v = \tilde{\delta}_v(t)$ and $\delta_c = \delta(t_{\rm surv})$. Equation (36) also defines the probability that a void merges into a system of volume larger than the corresponding volume scale $S_2$ at collapse barrier $\delta_c$. Then at collapse barrier $\delta_c$, this void collapses. Fig. 13 shows the collapse probabilities of embedded voids for given redshifts, when they incorporate into radius $R_2$ for the self-similar models. According to this, in all models, the collapse probability shows similar behaviour in terms of redshift. In other words, in a given model the probability distributions in terms of different redshifts slightly deviate from each other. In addition, in all models the collapse probabilities decrease with increasing size. This is an expected result since embedded/minor voids are to be affected by their environments. Embedded voids most likely collapse. Note that the radius range of the collapse probability distribution with value $P(R_2) = 1$ indicates 100 per cent success in collapsing. After the maximum collapse radius at a given redshift, the probability distribution starts decreasing towards large radii. Then it reaches the value zero indicating no collapse for voids in this radius at this given redshift. As a general feature of the models, the smallest size voids have the highest collapse probability. In addition, the size range of voids with highest collapse probability decreases with decreasing spectral index and also decreases towards higher redshift values in a given model. For example, in the self-similar models with index $n = 0, -1, -1.5$, voids with radius up to $\leq 4.5\,h^{-1}$ Mpc, $\leq 2.5\,h^{-1}$ Mpc and $\leq 1.5\,h^{-1}$ Mpc are destined to collapse at present-day $z_c = 0$. All voids with radii above these limits in the related model are less likely to collapse. The collapse radii with zero probability $P(R_2) = 0$ define the lowest radius limit of immortal voids that continuously grow/merge without collapsing. The radii of embedded voids that do not collapse ever, depending on the models are $\geq 65\,h^{-1}$ Mpc for $n = -1.5$, $\geq 35\,h^{-1}$ Mpc for $n = -1$ and $\geq 20\,h^{-1}$ Mpc for $n = 0$.

Apart from the collapse probability, the collapse failure rate of the embedded/minor void population is also defined. The collapse failure rate can be defined as the change of probability of a void that will not collapse at a given redshift interval. In other words, some embedded voids fail to collapse at a given redshift or a given size. The collapse failure rate is given by the negative signed derivative of the collapse probability in terms of $\delta_c$. Hence, the collapse failure rate of embedded/minor voids is given by,

$$F_{\delta_c,\rm coll} = {\rm d}\delta_c \left( \frac{\partial P(S \leq S_2, \delta_c | S_1, \tilde{\delta}_v)}{\partial \delta_c} \right) = \sqrt{\frac{2}{\pi}} {\rm e}^{-\frac{2}{3}\frac{S_1}{\delta_v^2} - y_n \frac{S_1^2}{\delta_v^4}} {\rm e}^{-\frac{(S_1-2S_2)^2}{2S_1S_2(S_1-S_2)}\delta_c^2} \frac{(S_1 - 2S_2)}{\sqrt{S_1 S_2 (S_1 - 2S_2)}}, \tag{38}$$

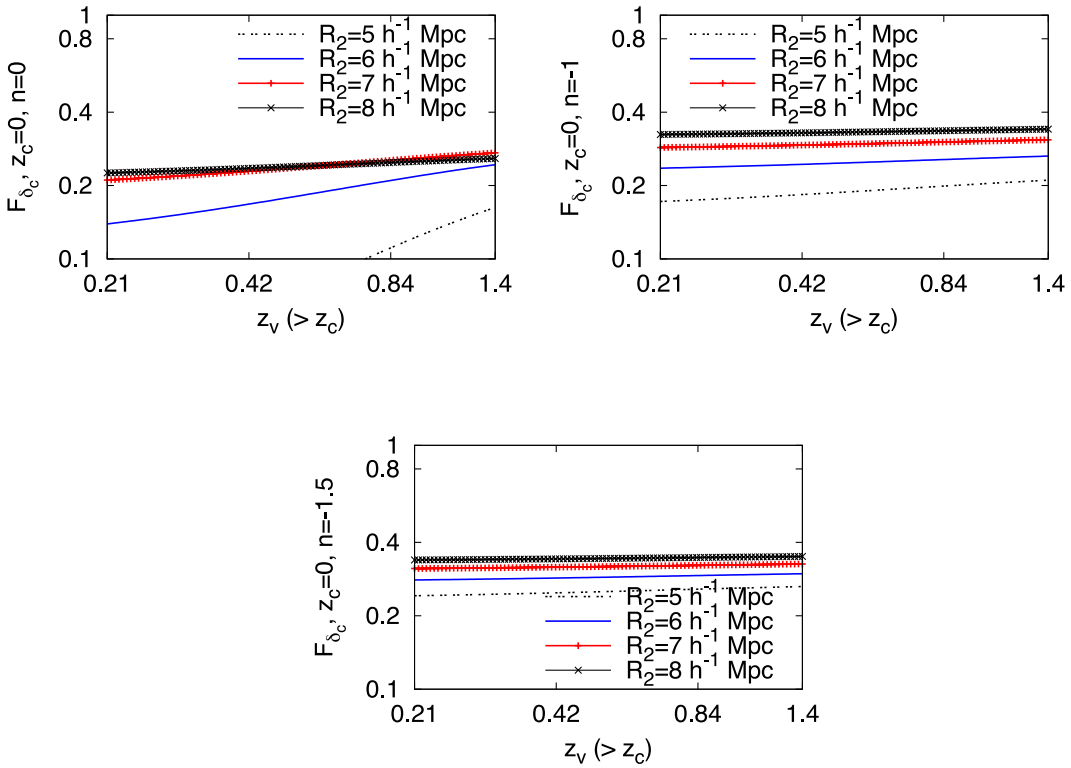


**Figure 14.** The failure rate of embedded voids in terms of merging redshift $z_v$ for given radii 5, 6, 7, 8 $h^{-1}$ Mpc in the self-similar models with index $n = 0$, $-1$, $-1.5$.

in which $y_n$ are the numerical values and given by values (37). Equation (38) then provides important information by showing at what redshift interval and what size of voids have chance to collapse or survive. Fig. 14 presents the collapse failure rates of embedded/minor voids in terms of redshift $z_v( > z_c = 0)$ for 5, 6, 7 and 8 $h^{-1}$ Mpc size voids. These embedded voids start merging at $z_v$ before reaching the collapse at redshift $z_c = 0$ in self-similar models based on equation (38). According to this, Fig. 14 demonstrates that the collapse failure rate slightly increases from $n = 0$ to $n = -1.5$ for a given size void. In addition to this, the failure rate becomes constant towards $n = -1.5$. According to this, relatively smaller size voids at high redshifts show lower collapse failure rate than their larger radius counterparts. While this behaviour is dominant in the self-similar-model $n = 0$, it becomes constant in redshift. However, smaller size embedded voids present smaller collapse failure rate. This shows that high redshifts keep slightly more small size voids rather than large ones.

Apart from the collapse failure rate of the void population in terms of redshift, it would be interesting to see the failure rate in terms of the size distribution for a given redshift range. Therefore, Fig. 15 shows the instantaneous probability of failing rate in terms of void radius $R_2$, in which a void doubles its size and collapses, for self-similar models with index $n = 0$, $-1$, $-1.5$. As is seen in the figure, the collapse failure rates are first increasing and then decreasing with increasing void radius at a given redshift in each model. This special shape of the collapse failure rate model is called the log normal survival model in the context of survival analysis (Kleinbaum & Klein 2011). In Fig. 15, the collapse failure rate of voids increases towards high redshifts. In the self-similar models, the collapse failure rates at given redshifts approach each other with decreasing spectral index. In addition, the failure rate increases with decreasing spectral index. However, in all models, the collapse failure rate increases until reaching a certain radius at a given redshift, then it starts decreasing. This means that in each redshift there is a characteristic (turn around) void radius that behaves as a transition criterion between collapsing and growing void radius. As a consequence of this, voids at their characteristic failure radius at a given redshift most likely dominate the void size distribution and they will dominate the given redshift. As is seen in Fig. 15, in the models, the peak of the failure rate increases with decreasing spectral index and decreasing redshift.

### 5.2 Volume formation time and extended void merging tree

Formation time for voids in the two-barrier excursion set is the same as growing voids in the one-barrier excursion set. Then, the formation time of a void is defined as the redshift at which a progenitor void of the main void forms with half of the volume of the main void. Following LC93, it is mentioned that after the formation time (or $S < S_1$), the choice of the largest volume progenitor as the main progenitor defines a continuous track through the merging tree. It is obvious that formation times have key importance in constructing a merging tree of voids. However, it is pointed out that obtaining formation times from random walks is problematic compared to obtaining the survival times since the volume assigned for a particle by tracking its density $\delta$ is not its actual volume but its approximate value (based on LC93). However, this fact does not lead to any self-inconsistency in merger rates and survival times. In addition to this, it has been shown that the analytical

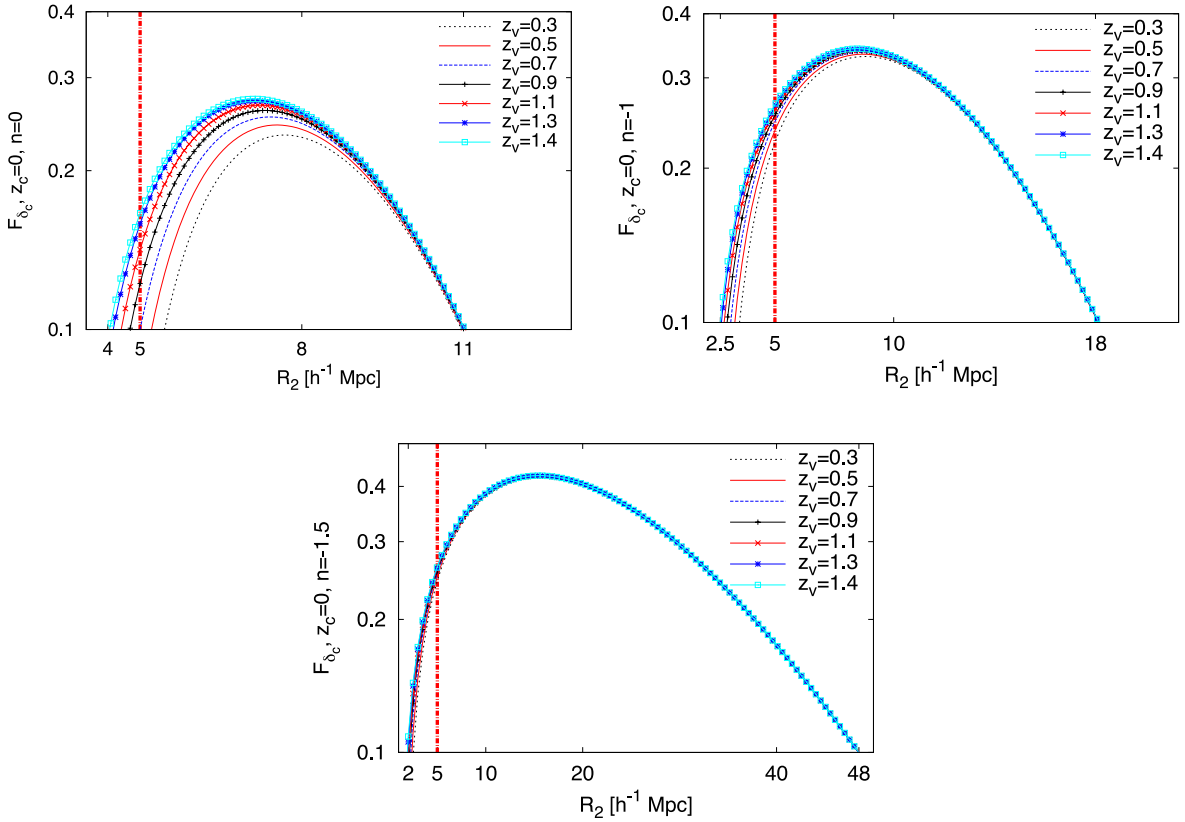


**Figure 15.** The failure rate of embedded/minor void regions in terms of the incorporated radius $R_2$ at given redshifts $z_v$ when voids start merging and they collapse at $z_c = 0$ in the self-similar models (with index $n = 0, -1, -1.5$ from upper to lower panels, respectively).

counting argument of generating merging histories provides similar results to LC93. The void counting method from the void perspective is discussed in the following.

### *5.2.1 Void counting, analytical method to extended void merging tree*

The void counting is based on defining the number density of voids in a given volume range. This number density evolves into a larger range at later times, which then allows us to obtain the probability distribution of voids with volume $V_2$ that had a parent in the volume range $V_2/2 < V_1 < V_2$ at $\tilde{\delta}_v$ and this probability equals the probability that its formation time is earlier than $\tilde{\delta}_v > \delta_f$. The counting method provides analytical solutions in terms of self-similar models which can be extended into the CDM model.

The number density of voids $(V_1, V_1 + \mathrm{d}V_1)$ at time $\tilde{\delta}_v$, which are incorporated into voids of volume $(V_2, V_2 + \mathrm{d}V_2)$ at time $\tilde{\delta}_v > \delta_c$ is

$$\mathrm{d}^2 n = \frac{\mathrm{d}n}{\mathrm{d}V_1}(V_1, \tilde{\delta}_v)\, \mathrm{d}V_1 f_{S_2}\left(S_2, \delta_c | S_1, \tilde{\delta}_v\right) \mathrm{d}S_2. \tag{39}$$

As long as $V_2 \leq V_1 < V_2/2$, each trajectory must connect unique voids because there cannot be two paths each of which contain more than half of the final volume. However, it is possible that the volume of void $V_2$ at $\delta_c$ has no progenitor of volume $< V_2/2$ at time $\tilde{\delta}_v$. The probability that a void with volume $V_2$ at $\delta_c$ has a progenitor in the volume range $V_2 > V_1 > V_2/2$ at time $\tilde{\delta}_v$ is then given by the ratio of voids that evolve to another volume $V_2$ relative to the total void volume $V_1$,

$$\frac{\mathrm{d}P\left(V_1, \tilde{\delta}_v | V_2, \delta_c\right)}{\mathrm{d}V_1} = \left(\frac{\mathrm{d}n(V_1)/\mathrm{d}V_1}{\mathrm{d}n(V_2)/\mathrm{d}V_2}\right) f_{S_1}\left(S_1, \tilde{\delta}_v | S_2, \delta_c\right) \left|\frac{\mathrm{d}S_1}{\mathrm{d}V_2}\right|, \tag{40}$$

which leads to

$$\frac{\mathrm{d}P\left(V_1, \tilde{\delta}_v | V_2, \delta_c\right)}{\mathrm{d}V_1} \mathrm{d}V_1 = \left(\frac{V_2}{V_1}\right) f_{S_1}\left(S_1, \tilde{\delta}_v | S_2, \delta_c\right) \mathrm{d}S_1. \tag{41}$$

Integration of equation (41) over the volume range $V_2/2 < V_1 < V_2$ gives the probability distribution of void $V_2$ that had a parent in this volume range at $\tilde{\delta}_v$, which equals the probability that its formation time is earlier than this,

$$\begin{aligned} P\left(\delta_f < \tilde{\delta}_v | V_2, \delta_c\right) &= P\left(V_1 < V_2/2 \tilde{\delta}_v | V_2, \delta_c\right) \\ &= \int_{S_2}^{S_h = S_2(V_2/2)} \left(\frac{V_2}{V_1}\right) f_{S_1}\left(S_1, \tilde{\delta}_v | S_2, \delta_c\right) \mathrm{d}S_1, \end{aligned} \tag{42}$$

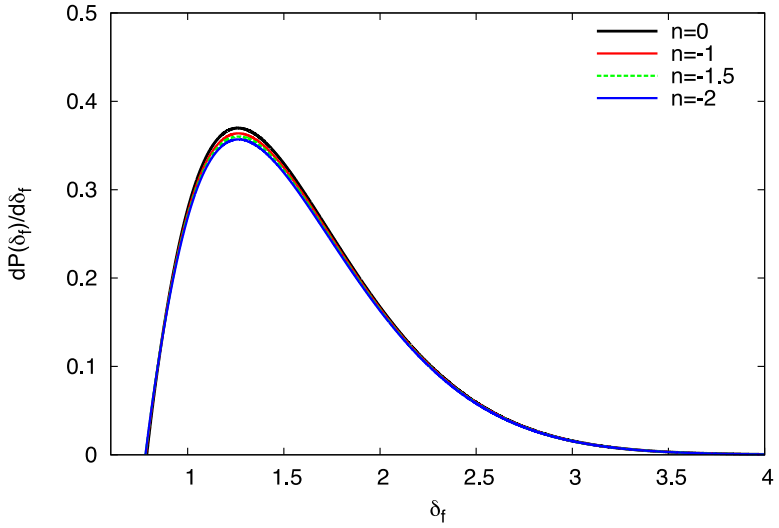


**Figure 16.** Numerical solution of the probability distribution of merging voids. This shows the distribution as a function of threshold height $\delta_f \sim z_f$ in terms of self-similar models. As is seen, the difference between models is small and negligible and the probability distributions of formation times form a peak around $\delta_f = 1.25$ for all self-similar models.

where $V_2/V_1$ is the weighting factor and $S_h = S(V_2/2)$. Volume ratios $V_2/V_1$ in the probability density function $f_{S_1}(S_1, \tilde{\delta}_v|S_2, \delta_c)$ define interval $[S_h, S_2]$. Therefore, in terms of self-similar models, the exact solutions of the probability function for $n = 0, -1.5, -2$ are derived for the spherical model (see A). In addition, probability (42) defines the distribution of formation times as well,

$$P\left(>\delta_f\right) = \int_0^1 \frac{1}{\sqrt{2\pi}} \left[\tilde{S}\left(2^\alpha - 1\right) + 1\right]^{1/\alpha} \frac{\delta_f}{\tilde{S}^{3/2}} \exp\left(-\frac{1}{2}\frac{\delta_f^2}{\tilde{S}}\right) \exp\left(-\frac{2}{9}\frac{\tilde{S}}{\delta_f^2} - \frac{32}{81}\frac{\tilde{S}^2}{\delta_f^4}\right) \mathrm{d}\tilde{S}, \tag{43}$$

by substituting the following transformations of $\tilde{S}$ and $\delta_f$, into the probability distribution (42),

$$\tilde{S} \equiv \frac{S - S_2}{S_h - S}, \qquad \delta_f \equiv \frac{\delta - \delta_c}{\sqrt{S_h - S_2}}. \tag{44}$$

For embedded voids, obtaining model-dependent analytical solutions is not possible. Therefore, the numerical solution of the merging probability (43) is investigated. Fig. 16 indicates the probability densities in terms of barrier height $\delta_f$ which is approximately the formation redshift $z_f$. This depicts the fact that the models have similar distributions and their difference is so small that it can be negligible.

## 6 SUMMARY AND DISCUSSION

In this study, the analytical growing void merging tree model of Russell (2013) based on the one-barrier excursion set/EPS formalism is extended to the two-barrier excursion set by taking into account collapsing subvoids as well as merging ones. To do this, excursion Brownian walk is constructed from the bridge-meander random walk of the void in cloud process by using a method given by Marchal (2003). This method allows one to use the two-barrier fraction function of void populations given by Sheth & van de Weygaert (2004). Then the merging tree algorithm of overdense regions derived by LC93 is modified into a void merging one in terms of the spherical model. A new parameter called the barrier height ratio $\gamma$ is defined, and this parameter is transformed into a new barrier height ratio $\tilde{\gamma}$ after the void and cloud process is treated to the cloud in cloud process. These barrier height ratios have key importance since they define the collapse and merging behaviours of the distribution function of the void population. Assuming spherical voids and binary merging which gives the relation of scales depending on the self-similar model $S_2 \approx 2^\alpha S_1$ and the barrier ratio $\tilde{\gamma} = 0.25$, the void merging algorithm for void populations is obtained in terms of the two-barrier EPS formalism. According to this, the following results are found.

(i) The size distribution of the embedded void populations are obtained by using the two-barrier EPS formalism. Making the distinction between growing and collapsing voids based on a choice of the barrier height ratio $\tilde{\gamma}$ (or $\gamma$) and the redshift constraints, it is shown that the size distribution of self-similar models present two cut-off values indicating the largest and smallest embedded voids at a given redshift. The cut-off sizes have the same lowest probabilities. In addition, the peak of a size distribution at a given redshift indicates that this size of embedded voids dominate the given epoch. The embedded voids with the highest distribution rate become smaller towards high redshifts. This behaviour corresponds to the fact that relatively small size embedded voids dominate the void distribution of the Universe at high redshifts compared to low-redshift values. This result agrees with hierarchical scenarios (Sheth & van de Weygaert 2004; Russell 2013; Ricciardelli, Quilis & Planelles 2013). On the other hand, observing of the largest spherical embedded voids is unlikely due to their low-probability values in the self-similar models. This theoretical result is in agreement with the observational and numerical study of Tavasoli et al. (2013). In Millennium I simulation mock data, Tavasoli et al. (2013) find that in the simulation, large voids are less abundant.

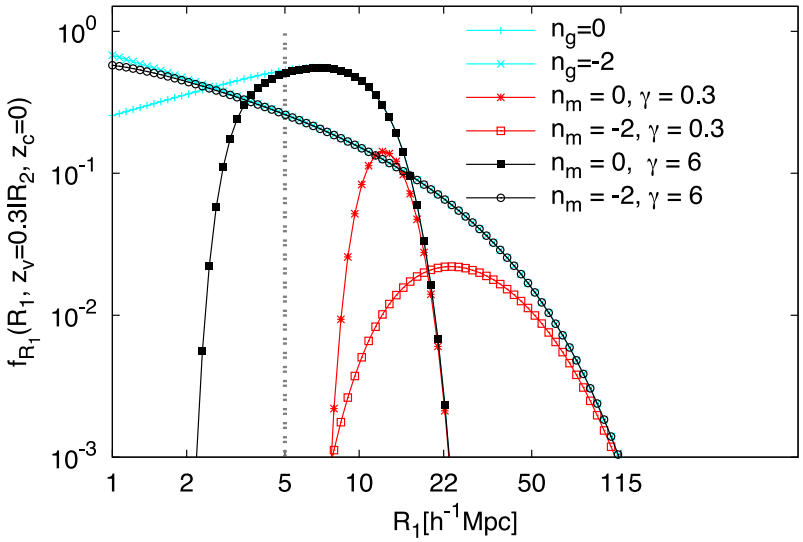


**Figure 17.** Comparison of the size distribution of void populations in terms of self-similar models with spectral indices $n_g = 0$ and $-2$ for growing and $n_m = 0$ and $-2$ for embedded/minor voids. In both models of size distribution of embedded/minor voids start merging events at $z_v = 0.3$ and collapse at present-day redshift $z_c = 0$. Growing voids only show merging behaviour since the collapse barrier is moved towards very high redshifts, in which the barrier ratio is chosen as $\gamma = 0.6$ and the merging redshift $z_v = 0$.

However, Sutter et al. (2013) point out the importance of the density of voids. Sutter et al. (2013) show that voids become larger, spherical and also small voids disappear when the tracer density is reduced. This is particulary interesting since void density is chosen as in the linear theory $\delta_v = -2.81$ in this study, based on Sheth & van de Weygaert (2004). Following up on the study of Sutter et al. (2013), the extended void merging algorithm should be tested for different underdensities based on the observational and numerical studies, in order to see how the embedded void algorithm changes.

In the extended void merging algorithm, it also is shown that the size of dominant embedded voids increases towards low spectral index while the size range of minor voids increases. This indicates that small scales are most likely dominated by larger size embedded voids than larger scales in the self-similar models.

The one-barrier excursion set formalism of growing voids of Russell (2013) shows slightly lower probability of sizes for a given model compared to the size distribution of growing voids that is obtained from the two-barrier EPS formalism by choosing $\delta_c \gg |\delta_v|$. However, the size distribution of growing voids of the two-barrier excursion set obtained from equation (27) for the barrier height ratio $\gamma \gg 0.5$ indicates smaller size voids than the size distribution function that is derived from the one-barrier excursion set formalism (Russell 2013). This is obviously because of the second barrier value in the conditional fractional function. In the one-barrier excursion set formalism, the second barrier in the conditional distribution function is a merging barrier $\delta_v$ while in the two-barrier approach, the second barrier in the conditional distribution function is the collapse barrier.

Fig. 17 explicitly represents this distinction between growing and embedded void populations with different spectral index. As was aforementioned, the void size distribution range increases with decreasing spectral index. As is seen in Fig. 17, this behaviour is more striking in a growing void size distribution than in embedded ones.

(ii) It is found that the merger rates of embedded voids that are derived in this paper and growing void populations of Russell (2013) are the same. Therefore, it can be concluded that embedded and growing void populations have the same merger characteristics. However, at some point embedded voids are destined to vanish or will be squeezed by the overdense regions while growing voids continuously merge. As an extension of this result and Russell (2013), it may be possible to generalize that embedded/minor and growing voids have the same merger rate characteristic as dark matter haloes.

(iii) The survival probability of the void population is defined and formulated analytically in terms of the two-barrier excursion set formalism. The two-barrier survival probability of the embedded/minor voids is named as the collapse probability. Then, a distinction between the survival probability of growing voids is made based on the one-barrier formalism and the collapse probability of the two-barrier formalism which has contributions from both the growing and the embedded void populations. According to this, while the survival probability of the growing void population is defined by the distribution of voids that will continue merging after reaching double their size, the collapse probability of embedded minor voids is defined as the probability of voids that merge until the collapse barrier/redshift.

In addition, it is shown that the collapse probability of embedded voids, that will vanish under collapse regions, indicates small void size ranges. This is due to the fact that large size/growing voids are not strongly affected by collapse regions (Sheth & van de Weygaert 2004; D'Aloisio & Furlanetto 2007; Ceccarelli et al. 2013; Russell 2013). Here, model-dependent upper limits on the radius of the embedded voids that will collapse with the highest probability $P_{\rm coll} = 1$ are obtained; these are $\leq$4.5 $h^{-1}$ Mpc, $\leq$2.5 $h^{-1}$ Mpc and $\leq$1.5 $h^{-1}$ Mpc for self-similar models with the index $n = 0, -1, -1.5$, respectively. Besides this, lower limits on the radius of embedded voids are calculated.

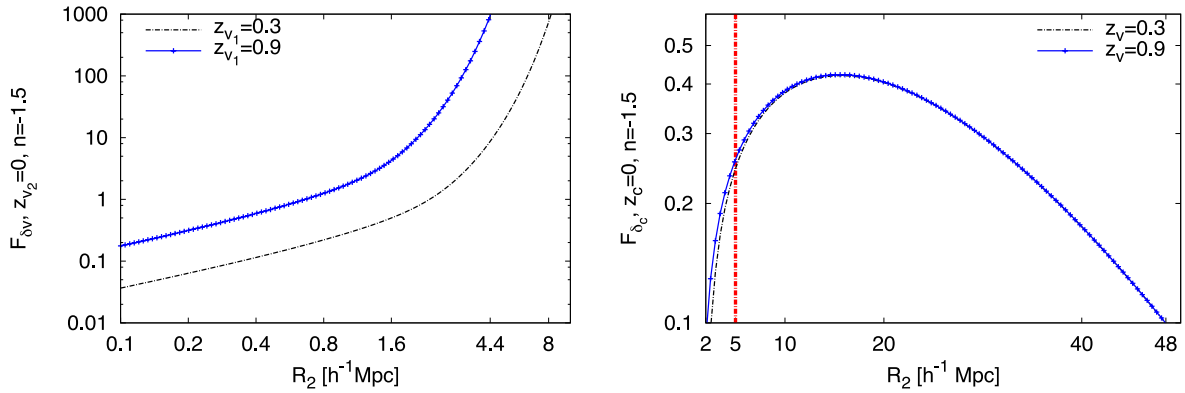


**Figure 18.** Comparison of the failure rates of growing (left) and embedded (right) voids for the self-similar model $n = -1.5$. These panels represent the failure rates of voids in terms of the one-barrier (left) and the two-barrier (right) EPS formalisms.

According to this, all voids with radii above these limits in the related model continuously grow/merge without collapsing. These lower limits are $\geq 20\ h^{-1}$ Mpc, $\geq 35\ h^{-1}$ Mpc and $\geq 65\ h^{-1}$ Mpc in the self-similar models with index $n = 0$, $-1$ and $-1.5$.

(iv) An analytical description of the collapse failure rate of the embedded voids is obtained. The collapse failure rate is defined as the change of probability of a void that will not collapse at a given redshift interval or size interval. According to this, the collapse failure rate of embedded voids is given by the negative derivative of the collapse probability distribution in terms of the collapse barrier/redshift $\delta_c \approx z_c$.

Consequently, it is shown that 5 $h^{-1}$ Mpc size embedded voids around $z_v = 1.4$ have more chance to collapse compared to large size $>5\ h^{-1}$ Mpc embedded voids. In the self-similar models, this tendency of collapsing of small size embedded voids reduces towards lower spectral indices. This may indicate that the collapse failure, or risk of an embedded void not collapsing, increases with increasing size. Given the definition of growing voids which do not collapse, this is an expected result and agrees with Sheth & van de Weygaert (2004); Russell (2013); Ceccarelli et al. (2013).

The failure rates of growing and embedded voids represent completely different behaviour. In Fig. 18, the comparison of the two different failure rate behaviours is given. According to this, the failure rate of growing voids measures the change in the probability distribution of a void which starts its evolution at merging barrier $\delta_{v_1} \approx z_{v_1}$ and later on incorporates its double size at a merging barrier $\delta_{v_2} \approx z_{v_2}$. The failure rate of embedded voids measures the change in the probability distribution of a void that starts merging at $\tilde{\delta_v} \approx z_v$ which then incorporates its double size and collapses at a collapse barrier $\delta_c \approx z_c$. Also, as is seen in Fig. 18, the shape of the collapse failure rate of the embedded voids is related to the log normal survival model, while only growing voids show the shape of another special failure rate called the Weibull survival model (Kleinbaum & Klein 2011) as is shown by Russell (2013). In addition, the failure rates for embedded voids increase up to a turnaround point at a certain radius at a given redshift. After these particular radii are reached, the failure rate starts decreasing. These turnaround void sizes in different models indicate the voids that have the most chance to survive without collapsing. Then the turnaround points of the failure rates give the size value of dominant embedded voids at a given redshift in the volume distribution.

(v) It is shown that although there are analytical solutions for the probability functions of void formation times in the one-barrier approach of Russell (2013), there are no analytical solutions for the expected void distribution in terms of the formation barrier based on the two-barrier formalism. Fig. 19 shows the comparison of the two- and one-barrier EPS formalism of void formation probability distributions for three different self-similar models. The two-barrier approach provides a better solution of the hierarchical void evolution than the one-barrier EPS formalism. The reason for this is the probability function of void formation times in the one-barrier EPS formalism has negative values

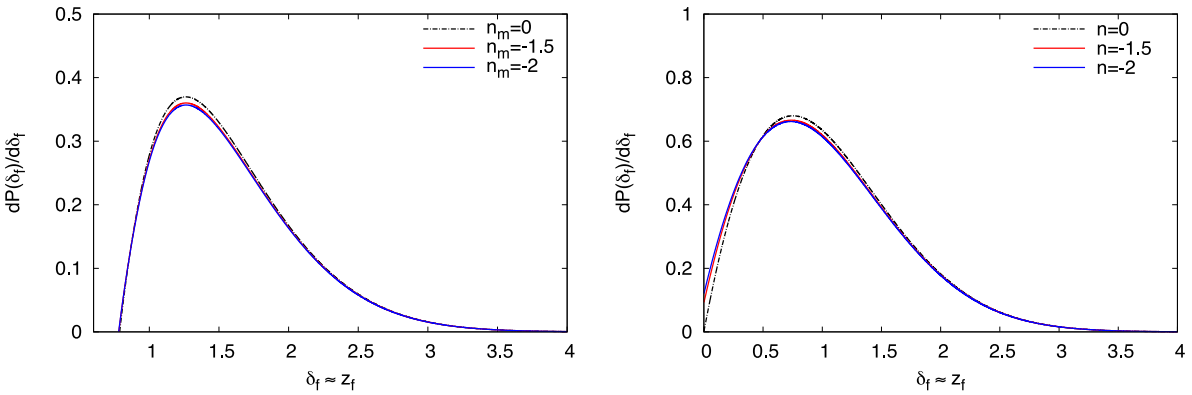


**Figure 19.** Comparison of numerical solutions of the probability distribution of formation times of voids in the two-barrier (left) and one-barrier (right) EPS formalisms in the self-similar models with spectral index $n = 0$, $-1.5$ and $-2$. In each plot, when the index decreases the probability distribution decreases as well. As can be seen, the difference between self-similar models in each plot is small.

for small formation barrier $\delta_f$ or redshift $z_f$, values which is not acceptable due to the definition of the probability function. However, the two-barrier approach does not have this problem. Nevertheless, the formation time distribution of the two-barrier approach is lower than the one-barrier one. This indicates that there are more void structures in the one-barrier EPS formalism than the two-barrier formalism.

As an extension of the one-barrier void merging tree algorithm of Russell (2013), here merging, survival, failure and formation time distributions of voids, that are embedded in overdense regions, are obtained. Also, this study only focuses on the self-similar models, which are approximated by a ΛCDM model by following Sheth & van de Weygaert (2004). Unlike the one-barrier void merging tree algorithm, the algorithm of the two-barrier void merging tree has complex mathematical derivations. Although its mathematical derivation is complex, it can be seen that its structure leads to the extension of the one-barrier void merging algorithm of Russell (2013).

The main goal of this paper is to provide a treatment of the void in cloud problem of the EPS formalism, and constructing an embedded void merging algorithm based on this new method. That is why, this extended void merging algorithm, focused on only the self-similar models in the case of spherical voids in the EdS Universe. As a result of this, collapse and expansion of a void are described in terms of linear theory, and the non-linear effects for smaller void sizes ($<5\ h^{-1}$ Mpc) in the void merging algorithm is neglected. However, it should be pointed out that when voids evolve in time, they tend to be more spherical (Centrella & Melott 1983; Fujimoto 1983; Bertschinger 1985) and this tendency is described by the Bubble Theorem of Icke (1984). Moreover, numerical studies show this tendency (Tavasoli et al. 2013) even for small-scale subvoids (Ricciardelli et al. 2013). On the other hand, Jennings, Li & Hu (2013) obtain the number density of spherical voids using a linearly extrapolated density $\delta_v = -2.7$ in the dark matter distribution from *N*-body simulations in a ΛCDM cosmology. They show that the abundance of voids at redshift $z = 0$ does not match the abundance given by Sheth & van de Weygaert (2004). Jennings et al. (2013) stress the fact that the EPS formalism of Sheth & van de Weygaert (2004) does not take into account merging of voids as they expand. Note that here we investigate only the self-similar spectra to construct a void merging algorithm which is based on the LC93 dark matter merging algorithm. LC93 merging tree algorithm of dark matter haloes is limited to the self-similar models and provides an approximated dark matter solutions. That is why, investigating the extended void merging algorithm in different ΛCDM models by using different CDM power spectra and taking into account non-linear effects on small-size voids seem essential in order to achieve a proper full understanding of the formation and dynamics of the Cosmic Web from a void-based structure formation. As a result, the extended and growing void merging algorithms can be tested and then may provide a realistic framework. Therefore, the ΛCDM models and non-linear effects on small-size voids in these void merging algorithms will be discussed in detail in a follow-up paper.

## ACKNOWLEDGEMENT

ER would like to sincerely thank, the referee, Dr. Basilakos for his insightful comments and suggestions which improve this study constructively.

## REFERENCES

Aragon-Calvo M. A., Szalay A. S., 2013, MNRAS, 428, 3409
Benson A. J., Hoyle F., Torres F., Vogeley M. S., 2003, MNRAS, 340, 160
Bertschinger E., 1985, ApJS, 58, 1
Beygu B., Kreckel K., van de Weygaert R., van der Hulst J. M., van Gorkom J. H., 2013, AJ, 145, 120
Blumenthal G. R., da Costa L. N., Goldwirth D. S., Lecar M., Piran T., 1992, ApJ, 388, 234
Bond J. R., Cole S., Efstathiou G., Kaiser N., 1991, ApJ, 379, 440
Bond J. R., Kofman L., Pogosyan D., 1996, Nature, 380, 603
Bos E. G. P., van de Weygaert R., Dolag K., Pettorino V., 2012, MNRAS, 426, 440
Brookfield A. W., van de Bruck C., Hall L. M. H., 2008, Phys. Rev. D, 77, 043006
Ceccarelli L., Paz D., Lares M., Padilla N., Lambas D. G., 2013, MNRAS, 434, 1435
Centrella J., Melott A. L., 1983, Nature, 305, 196
Clampitt J., Cai Y.-C., Li B., 2013, MNRAS, 431, 749
Colberg J. M., Sheth R. K., Diaferio A., Gao L., Yoshida N., 2005, MNRAS, 360, 216
Colberg J. M. et al., 2008, MNRAS, 387, 933
D'Aloisio A., Furlanetto S. R., 2007, MNRAS, 382, 860
D'Amico G., Musso M., Noreña J., Paranjape A., 2011, Phys. Rev. D, 83, 023521
da Costa L. N. et al., 1994, ApJ, 424, L1
Dubinski J., da Costa L. N., Goldwirth D. S., Lecar M., Piran T., 1993, in Chincarini G. L., Iovino A., Maccacaro T., Maccagni D., eds, ASP Conf. Ser. Vol. 51, Observational Cosmology. Astron. Soc. Pac., San Francisco, p. 188
Einasto M., Tago E., Jaaniste J., Einasto J., Andernach H., 1997, A&AS, 123, 119
El-Ad H., Piran T., Dacosta L. N., 1997, MNRAS, 287, 790
Farrar G. R., Peebles P. J. E., 2004, ApJ, 604, 1
Farrar G. R., Rosen R. A., 2007, Phys. Rev. Lett., 98, 171302
Fisher K. B., Huchra J. P., Strauss M. A., Davis M., Yahil A., Schlegel D., 1995, ApJS, 100, 69
Fitzsimmons P., Pitman J., Yor M., 1993, in Cinler E., Chung K. L., J. S. M., eds, Seminar on Stochastic Processes Markovian bridges: Construction, Palm interpretation, and Splicing. Springer-Verlag, Berlin, p. 101
Fujimoto M., 1983, PASJ, 35, 159
Furlanetto S. R., Piran T., 2006, MNRAS, 366, 467
Geller M. J., Huchra J. P., 1989, Science, 246, 897

Gottlöber S., Łokas E. L., Klypin A., Hoffman Y., 2003, MNRAS, 344, 715
Gubser S. S., Peebles P. J. E., 2004a, Phys. Rev. D, 70, 123511
Gubser S. S., Peebles P. J. E., 2004b, Phys. Rev. D, 70, 123510
Hellwing W. A., Juszkiewicz R., 2009, Phys. Rev. D, 80, 083522
Hoyle F., Vogeley M. S., 2002, ApJ, 566, 641
Hoyle F., Vogeley M. S., 2004, ApJ, 607, 751
Icke V., 1984, MNRAS, 206, 1 P
Jennings E., Li Y., Hu W., 2013, MNRAS, 434, 2167
Jõeveer M., Einasto J., Tago E., 1978, MNRAS, 185, 357
Jones D. H. et al., 2004, MNRAS, 355, 747
Karachentsev I. D., Karachentseva V. E., Huchtmeier W. K., Makarov D. I., 2004, AJ, 127, 2031
Kirshner R. P., Oemler A., Jr, Schechter P. L., Shectman S. A., 1981, ApJ, 248, L57
Kleinbaum D. G., Klein M., 2011, Survival Analysis: A Self-Learning Text. Springer-Verlag, Berlin
Kraan-Korteweg R. C., Shafi N., Koribalski B. S., Staveley-Smith L., Buckland P., Henning P. A., Fairall A. P., 2008, in Jerjen H., Koribalski B. S., eds, Outlining the Local Void with the Parkes HI ZOA and Galactic Bulge Surveys. Springer-Verlag, Berlin, p. 13
Kreckel K., Joung M. R., Cen R., 2011, ApJ, 735, 132
Kreckel K., Platen E., Aragón-Calvo M. A., van Gorkom J. H., van de Weygaert R., van der Hulst J. M., Beygu B., 2012, AJ, 144, 16
Lacey C., Cole S., 1993, MNRAS, 262, 627 (LC93)
Lavaux G., Wandelt B. D., 2010, MNRAS, 403, 1392
Lavaux G., Wandelt B. D., 2012, ApJ, 754, 109
Marchal P., 2003, in Banderier C., Krattenthaler C., eds, Proc. Discrete Mathematics and Theoretical Computer Science, Discrete Random Walks DRW'03. p. 181
Mathis H., White S. D. M., 2002, MNRAS, 337, 1193
Maurogordato S., Schaeffer R., da Costa L. N., 1992, ApJ, 390, 17
Pan D. C., Vogeley M. S., Hoyle F., Choi Y.-Y., Park C., 2012, MNRAS, 421, 926
Paranjape A., Lam T. Y., Sheth R. K., 2012, MNRAS, 420, 1648
Pitman J., 1999, Electron. J. Probab., 4, 1
Plionis M., Basilakos S., 2002, MNRAS, 330, 399
Press W. H., Schechter P., 1974, ApJ, 187, 425
Regos E., Geller M. J., 1991, ApJ, 377, 14
Ricciardelli E., Quilis V., Planelles S., 2013, MNRAS, 434, 1192
Russell E., 2013, MNRAS, 436, 3525
Sahni V., Sathyaprakah B. S., Shandarin S. F., 1994, ApJ, 431, 20
Saunders W. et al., 2000, MNRAS, 317, 55
Shang C., Crotts A., Haiman Z., 2007, ApJ, 671, 136
Shectman S. A., Landy S. D., Oemler A., Tucker D. L., Lin H., Kirshner R. P., Schechter P. L., 1996, ApJ, 470, 172
Sheth R. K., van de Weygaert R., 2004, MNRAS, 350, 517
Strauss M. A., Davis M., Yahil A., Huchra J. P., 1992, ApJ, 385, 421
Sutter P. M., Lavaux G., Wandelt B. D., Weinberg D. H., 2012a, ApJ, 761, 44
Sutter P. M., Lavaux G., Wandelt B. D., Weinberg D. H., 2012b, ApJ, 761, 187
Sutter P. M., Lavaux G., Wandelt B. D., Hamaus N., Weinberg D. H., Warren M. S., 2013, preprint (arXiv:1309.5087)
Tavasoli S., Vasei K., Mohayaee R., 2013, A&A, 553, A15
Tikhonov A. V., Karachentsev I. D., 2006, ApJ, 653, 969
Tikhonov A. V., Klypin A., 2009, MNRAS, 395, 1915
Tikhonov A. V., Gottlöber S., Yepes G., Hoffman Y., 2009, MNRAS, 399, 1611
Tinker J. L., Conroy C., 2009, ApJ, 691, 633
Tully R. B., Shaya E. J., Karachentsev I. D., Courtois H. M., Kocevski D. D., Rizzi L., Peel A., 2008, ApJ, 676, 184
van de Weygaert M. A. M., 1991, PhD thesis, Univ. Leiden
van de Weygaert R., 2003, Eric D. F., Babu G. J. eds., SCMA III Conf., The Cosmic Foam: Stochastic Geometry and Spatial Clustering Across the Universe. Springer, New York, p. 175
van de Weygaert R., Bond J. R., 2008, in Plionis M., López-Cruz O., Hughes D., eds, Lecture Notes in Physics, Vol. 740, A Pan-Chromatic View of Clusters of Galaxies and the Large-Scale Structure. Springer-Verlag, Berlin, p. 409
van de Weygaert R., Platen E., 2011, Int. J. Mod. Phys., 1, 41
van de Weygaert R., van Kampen E., 1993, MNRAS, 263, 481
Vervaat W., 1979, Ann. Probab., 1, 143
Viel M., Colberg J. M., Kim T.-S., 2008, MNRAS, 386, 1285

## APPENDIX A: ANALYTICAL DERIVATIONS IN THE EXTENDED VOID MERGING TREE

The probability of an embedded void forming at $\delta_f \approx z_f$, that later on doubles its volume and collapses at the barrier $\delta_c \approx z_c$, is given by

$$P\left(\delta_f < \tilde{\delta}_v | V_2, \delta_c\right) = P\left(V_1 < V_2/2\tilde{\delta}_v | V_2, \delta_c\right) = \int_{S_2}^{S_h = S_2(V_2/2)} \left(\frac{V_2}{V_1}\right) f_{S_1}\left(S_1, \tilde{\delta}_v | S_2, \delta_c\right) \mathrm{d}S_1.$$

In self-similar models with index $n = 1, 0, -1.5$ and $-2$, the exact solutions of the probability function are obtained for the spherical model as

$$P_{n=1} = \tilde{\Omega}_1 \frac{5}{6}\left[\mathrm{erf}\left(\sqrt{\frac{5}{6}}\frac{\tilde{k}}{\sqrt{S_h}}\right) - \mathrm{erf}\left(\sqrt{\frac{5}{6}}\frac{\tilde{k}}{\sqrt{S_2}}\right)\right] \tag{A1}$$

$$P_{n=0} = \tilde{\Omega}_0(S_2)\frac{\tilde{k}}{S_2}\left[\mathrm{erf}\left(\frac{\tilde{k}}{\sqrt{2}\sqrt{S_h - S_2}}\right)\left(\tilde{k} - \frac{S_2}{\tilde{k}}\right) - \sqrt{\frac{2}{\pi}}\sqrt{S_h - S_2}e^{\frac{-\tilde{k}^2}{(S_h - S_2)}}\right] \tag{A2}$$

$$P_{n=-1.5} = \tilde{\Omega}_{-1.5}(S_2)\frac{\tilde{k}}{S_2^2}\left(\mathrm{erf}\left(\frac{\tilde{k}}{\sqrt{2}\sqrt{S_h - S_2}}\right)\left(2\tilde{k}S_2 - \frac{\tilde{k}^3}{3} - \frac{S_2^2}{\tilde{k}}\right) + \frac{1}{3}\sqrt{\frac{2}{\pi}}\sqrt{S_h - S_2}\left(S_h + 5S_2 - \tilde{k}^2\right)\mathrm{e}^{-\frac{\tilde{k}^2}{2(S_h - S_2)}}\right) \tag{A3}$$

$$\begin{aligned} P_{n=-2} = {} & \tilde{\Omega}_{-2}(S_2)\frac{\tilde{k}}{S_2^3}\left(\mathrm{erf}\left(\frac{\tilde{k}}{\sqrt{2}\sqrt{S_h - S_2}}\right)\left(\frac{\tilde{k}^5}{15} - \tilde{k}^3 S_2 + 3\tilde{k}S_2^2 - \frac{S_2^3}{\tilde{k}}\right) + \frac{1}{15}\sqrt{\frac{2}{\pi}}\sqrt{S_h - S_2}\right. \\ & \left.\times\left(\tilde{k}^4 - \tilde{k}^2 S_h + 3S_h^2 + S_2(9S_h - 14\tilde{k}^2) + 33S_2^2\right)\mathrm{e}^{-\frac{\tilde{k}^2}{2(S_h - S_2)}}\right), \end{aligned} \tag{A4}$$

where $e$ stands for the exponential function while $\tilde{k}$ and $\tilde{\Omega}(S_2)$ are defined as

$$\tilde{k} \equiv \tilde{\delta}_v - \delta_c,$$

$$\tilde{\Omega}_1(S_2) \equiv \mathrm{e}^{-\frac{4}{3}\frac{S_2}{\delta_v^2} - 14.222\frac{S_2^2}{\delta_v^4}}, \qquad \tilde{\Omega}_0(S_2) \equiv \mathrm{e}^{-\frac{4}{3}\frac{S_2}{\delta_v^2} - 11.061\frac{S_2^2}{\delta_v^4}},$$

$$\tilde{\Omega}_{-1.5}(S_2) \equiv \mathrm{e}^{-\frac{4}{3}\frac{S_2}{\delta_v^2} - 6.614\frac{S_2^2}{\delta_v^4}}, \qquad \tilde{\Omega}_{-2}(S_2) \equiv \mathrm{e}^{-\frac{4}{3}\frac{S_2}{\delta_v^2} - 6.121\frac{S_2^2}{\delta_v^4}}. \tag{A5}$$

This paper has been typeset from a TEX/LATEX file prepared by the author.